This article has original data in the JCB Data Viewer

http://jcb-dataviewer.rupress.org/jcb/browse/5425

FGFR1 cleavage and nuclear translocation regulates breast cancer cell behavior

Athina-Myrto Chioni and Richard Grose

Centre for Tumour Biology, Barts Cancer Institute—A Cancer Research UK Centre of Excellence, Queen Mary University of London, London EC1M 6BQ, England, UK

FGF-10 and its receptors, FGFR1 and FGFR2, have been implicated in breast cancer susceptibility and progression, suggesting that fibroblast growth factor (FGF) signaling may be co-opted by breast cancer cells. We identify a novel pathway downstream of FGFR1 activation, whereby the receptor is cleaved and traffics to the nucleus, where it can regulate specific target genes. We confirm Granzyme B (GrB) as the protease responsible for cleavage and show that blocking GrB activity stopped FGFR1 trafficking to the nucleus and abrogates the promigratory effect of FGF stimulation. We confirm the in vivo relevance of our findings, showing that FGFR1 localized to the nucleus specifically in invading cells in both clinical material and a three-dimensional model of breast cancer. We identify target genes for FGFR1, which exert significant effects on cell migration and may represent an invasive signature. Our experiments identify a novel mechanism by which FGF signaling can regulate cancer cell behavior and provide a novel therapeutic target for treatment of invasive breast cancer.

Introduction

FGF receptors (FGFRs), as members of the receptor tyrosine kinase (RTK) family, are known to signal, after ligand binding and receptor dimerization, from the cell membrane as well as from endosomal compartments (Sorokin et al., 1994; Eswarakumar et al., 2005; Kermorgant and Parker, 2008). Signal transduction, primarily through the MAPK pathway but also acting via phosphoinositide 3-kinase (PI3K), PLC-γ, and STATs (Corson et al., 2003; Dailey et al., 2005), results in activation of several known target genes (e.g., *CyclinD1* and *PEA3*) to modulate cell behavior (Ho and Dowdy, 2002; Chioni and Grose, 2009). In addition to these well-studied signaling pathways, there is a growing body of evidence showing that full-length FGFRs, and FGFR1 in particular, can be targeted to the nucleus (Maher, 1996; Stachowiak et al., 1996a,b; Peng et al., 2001, 2002; Hu et al., 2004; Bryant et al., 2005). Relatively few studies have addressed the mechanism by which full-length RTKs translocate from the cell membrane to the nucleus (Stachowiak et al., 1996a, 2007; Reilly and Maher, 2001; Peng et al., 2002; Hu et al., 2004; Reilly et al., 2004); however, there is

a model emerging whereby, upon ligand binding, activated receptors are internalized to the early endosome compartment (Bryant and Stow, 2005; Bryant et al., 2005). Although FGF ligands are known to exit the endosome by a mechanism dependent on vesicular transmembrane potential (Małecki et al., 2002), how the receptors escape is unclear. Once in the cytoplasm, full-length FGFR1 has been shown to use the Importin β pathway to enter the nucleus (Reilly and Maher, 2001), where the receptor can interact with nuclear proteins to regulate transcription (Wiedłocha et al., 1994; Hu et al., 2004).

An alternative, and more intuitive, model for the nuclear trafficking of receptors is that activation-dependent cleavage of the intracellular domain allows the free cytoplasmic portion to translocate to the nucleus without a full-length receptor having to extract itself from the lipid bilayer. This mechanism is well known for Notch signaling (Bray, 2006) but has been shown for other receptors; these include ErbB4, which also undergoes ADAM-mediated ectodomain cleavage before γ-secretase cleavage and subsequent nuclear translocation (Carpenter and Liao, 2009). However, to date, there are no data suggesting that a similar proteolytic pathway might play a role in FGFR signaling, although, interestingly, FGFR1 has

Supplemental Material can be found at:
http://jcb.rupress.org/content/suppl/2012/05/31/jcb.201108077.DC1.html
Original image data can be found at:
http://jcb-dataviewer.rupress.org/jcb/browse/5425

The Rockefeller University Press $30.00
J. Cell Biol. Vol. 197 No. 6   801–817
www.jcb.org/cgi/doi/10.1083/jcb.201108077

JCB   801

been identified previously as a substrate for Granzyme B (GrB)–mediated cleavage (Loeb et al., 2006).

With evidence increasing that other RTKs play a functional role in the nucleus (Wang et al., 2010), we show here, for the first time, that a C-terminal fragment of FGFR1, generated by receptor activation-dependent cleavage, traffics to the nucleus and regulates the expression of target genes. We confirm GrB as the protease that mediates cleavage and show that GrB inhibition can block specific FGF-dependent effects on cancer cells. Having identified a functional role for nuclear FGFR1 in 2D and 3D cell culture models, we show that this phenomenon also occurs in vivo in invasive breast cancer and have identified a panel of FGFR1-regulated target genes, all of which regulate cell migration and thus could reflect an invasive signature.

The FGFR signaling pathway is implicated in a wide range of pathologies, most notably cancer (Turner and Grose, 2010), yet its efficient targeting is proving challenging to the pharmaceutical industry, partly because FGFR signaling is fundamental to so many normal biological processes. Our data suggest that targeting GrB rather than FGFR1 might represent a novel therapeutic approach in blocking cancer invasion.

Results

Expression and activation of FGFR1 and its biochemical and functional consequences

To ensure that our breast cancer cell lines exhibited a standard response to FGF-10 stimulation, serum-starved MCF-7 cells were stimulated with 100 ng/ml FGF-10 in the presence of 300 ng/ml heparin in serum-free media for 15, 30, and 60 min. Western blotting using antibodies specific to phosphorylated FRS2, extracellular signal–regulated kinase (ERK), AKT, and PLC-γ confirmed that stimulation with FGF-10 activated the FRS2 ERK pathway as well as the AKT pathway in MCF-7 cells (Fig. 1 A). FGF-10 treatment triggered rapid ERK phosphorylation, and this response was blocked by pretreatment with the FGFR inhibitor, PD173074 (2 µM; 1 h; Fig. 1 A). Other pathways (PLC-γ and PI3K) were investigated also, but although FGF-10 induced AKT phosphorylation, this was only partially reduced by treatment with PD173074 (Fig. 1 A).

To confirm that our cell lines behaved as expected after FGF-10 treatment, we performed a series of functional assays. Migration of MCF-7 and MDA-MB-231 cells was monitored using 8-µm-pore Transwell migration filters in a 24-well plate format overnight in serum-free medium in the presence or absence of FGF-10/heparin and/or PD173074 (Fig. 1 B). FGF-10 treatment increased Transwell migration of both MCF-7 and MDA-MB-231 cells significantly, and this effect was blocked in the presence of PD173074 (Fig. 1 B).

To confirm that the effect of FGF-10 on migration was a result of more cells migrating through the Transwell membrane and not caused by cell proliferation and/or cell death, cells were plated in 24-well plates in serum-free media (with or without FGF-10/heparin and/or PD173074) and counted after 12, 24, and 48 h (unpublished data). FGF-10 treatment

(in serum-free medium) increased cell number significantly in MCF-7 cells only after 48 h. However, there was no change in cell number with any of the treatments during the course of the Transwell migration assays. Cells were stained with an anti-Ki67 antibody to quantify cell proliferation. FGF-10 treatment resulted in a significant increase, after 48 h, in the percentage of MCF-7 cells staining positive for the proliferation marker Ki67 (Fig. 1 C). Moreover, FGF-10 treatment reduced apoptosis in MCF-7 cells after 48 h as determined by TUNEL assay (Fig. 1 D).

Subcellular localization of FGFR1

FGF-10 treatment (60 min) of serum-starved MCF-7 and MDA-MB-231 cells resulted in dramatically increased nuclear localization of FGFR1 immunostaining (Fig. 2 A and Fig. S1 A). This effect was abolished in the presence of the PD173074 inhibitor (Fig. 2 A); hence, the phenomenon was FGFR signaling specific. The results were reproduced independently (Fig. S1 A) using anti-FGFR1 antibodies specific for the C terminus and juxtamembrane regions of human FGFR1 (Santa Cruz Biotechnology, Inc. and Abcam, respectively). A z scan of images taken with both anti-FGFR1 antibodies showed that FGFR1 was within the nucleus (Fig. 2 A and Fig. S1 B).

To validate the antibodies used for detecting FGFR1 in immunofluorescence and Western blotting, we knocked down FGFR1 expression using RNAi (Fig. S1, C and D). MCF-7 and MDA-MB-231 cells, treated with a scrambled RNAi control or FGFR1-specific RNAi, showed significantly reduced FGFR1 mRNA expression as determined by real-time RT-PCR (Fig. S1 C). This knockdown of expression also was evident at the protein level, with control MCF-7 cells showing clear staining for FGFR1, in contrast to the absence of staining in cells treated with FGFR1 RNAi (Fig. S1 D). In addition, Western blotting also detected a significant reduction of FGFR1 after RNAi treatment (Fig. S1 D). The FGFR1 signal in Western blotting was eliminated by preincubation with an immunizing peptide (unpublished data).

To confirm immunofluorescence findings, subcellular fractionation and Western blotting on MCF-7 cells were performed after FGF-10 stimulation. Four fractions were obtained (cytoplasm, plasma membrane/organelles, nucleus, and cytoskeleton), revealing full-length FGFR1 (∼120 kD) in the plasma membrane/organelle fraction and a truncated FGFR1 fragment (∼55–60 kD) in the nuclear fraction (Fig. 2 B). Both the nuclear FGFR1 and full-length FGFR1 bands disappeared after preincubation of the anti-FGFR1 antibody with the immunizing peptide (unpublished data). FGF-10 stimulation of MCF-7 cells (0–60 min) caused a significant increase in accumulation of the truncated 55-kD C-terminal fragment of FGFR1 in the nuclear fraction (Fig. 2 B). Normalization to the nuclear marker TOPOIIa highlighted the significance of the nuclear FGFR1 accumulation (Fig. 2 B, graph). Immunoblotting with TOPOIIa and BIP antibodies confirmed the specificity of the cell fractionation protocol, and pERK confirmed successful FGF-10 stimulation (Fig. 2 B). Similar results were obtained with MDA-MB-231 cells (unpublished data).
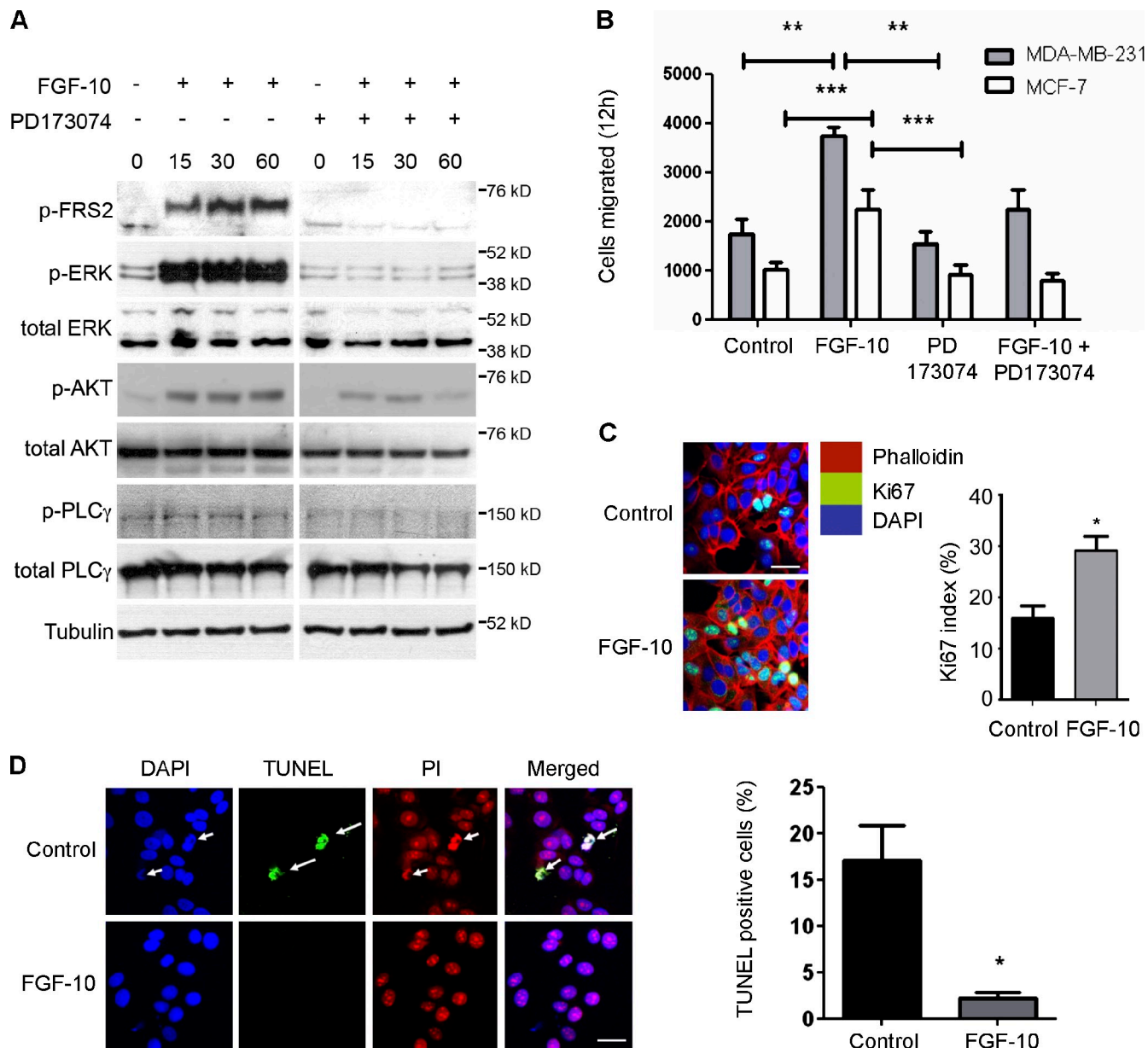
A

B

C

D

Figure 1.   **Cell signaling pathways activated upon FGF-10 stimulation and their impact on cell behavior.** (A) Serum-starved MCF-7 cells were stimulated with 100 ng/ml FGF-10 in the presence of 7.5 µg/ml heparin in serum-free media for 15, 30, and 60 min. Where indicated, cells were pretreated with 2 µM PD173074 (1 h). Cell lysates were prepared, and Western blotting was performed using different primary antibodies. Stimulation with FGF-10 activated the FRS2–ERK pathway as well as the AKT pathway. FGF-10 treatment triggered rapid ERK phosphorylation, which was blocked by the FGFR inhibitor PD173074. Other pathways (PLC-γ and PI3K) were also investigated, but although FGF-10 induced AKT phosphorylation, this was not abrogated by treatment with PD173074. PLC-γ was not activated by FGF-10 treatment. (B) Migration of MCF-7 and MDA-MB-231 cells was monitored using 8-µm-pore Transwell migration filters in serum-free medium in the presence of FGF-10/heparin (100 ng/ml and 7.5 µg/ml, respectively) and/or 2 µM PD173074. Cells were allowed to migrate overnight. FGF-10 treatment increased Transwell migration significantly, and this effect was blocked in the presence of the PD173074. (C) Immuno-staining with an anti-Ki67 antibody to quantify cell proliferation after 48 h revealed that treatment with FGF-10 resulted in a significant increase in the percent-age of positive cell staining. (D) FGF-10 treatment reduced apoptosis in MCF-7 cells after 48-h treatment with FGF-10, as determined by TUNEL assay (PI, propidium iodide). *, $P \leq 0.05$; **, $P \leq 0.01$; ***, $P \leq 0.001$ (ANOVA for B; Student's t test for C and D). Bars, 25 µm. Error bars show means ± SEM.

Cleavage of FGFR1 by GrB

FGFR1 previously has been identified as a substrate for GrB (Loeb et al., 2006), and a schematic representation of FGFR1 depicting the GrB cleavage site at Asp-432 is shown (Fig. 3 A). Western blot analysis with an anti-GrB antibody confirmed GrB expression in MCF-7 cells (Fig. 3).

Confocal analysis of MCF-7 cells treated with GrB RNAi for 72 h revealed efficient knockdown of GrB, concomitant with

decreased nuclear FGFR1 staining (Fig. 3 B). Western blot analysis also showed that 72-h treatment with RNAi to GrB reduced levels of nuclear FGFR1, despite an overall increase in full-length FGFR1 (Fig. 3 C). Efficiency of GrB knockdown was analyzed both by immunofluorescence and Western blotting (Fig. 3, B and C).

Subcellular fractionation and confocal analysis revealed that, similar to GrB RNAi, treatment with a GrB inhibitor blocked the capacity of FGF-10 to induce nuclear localization of FGFR1
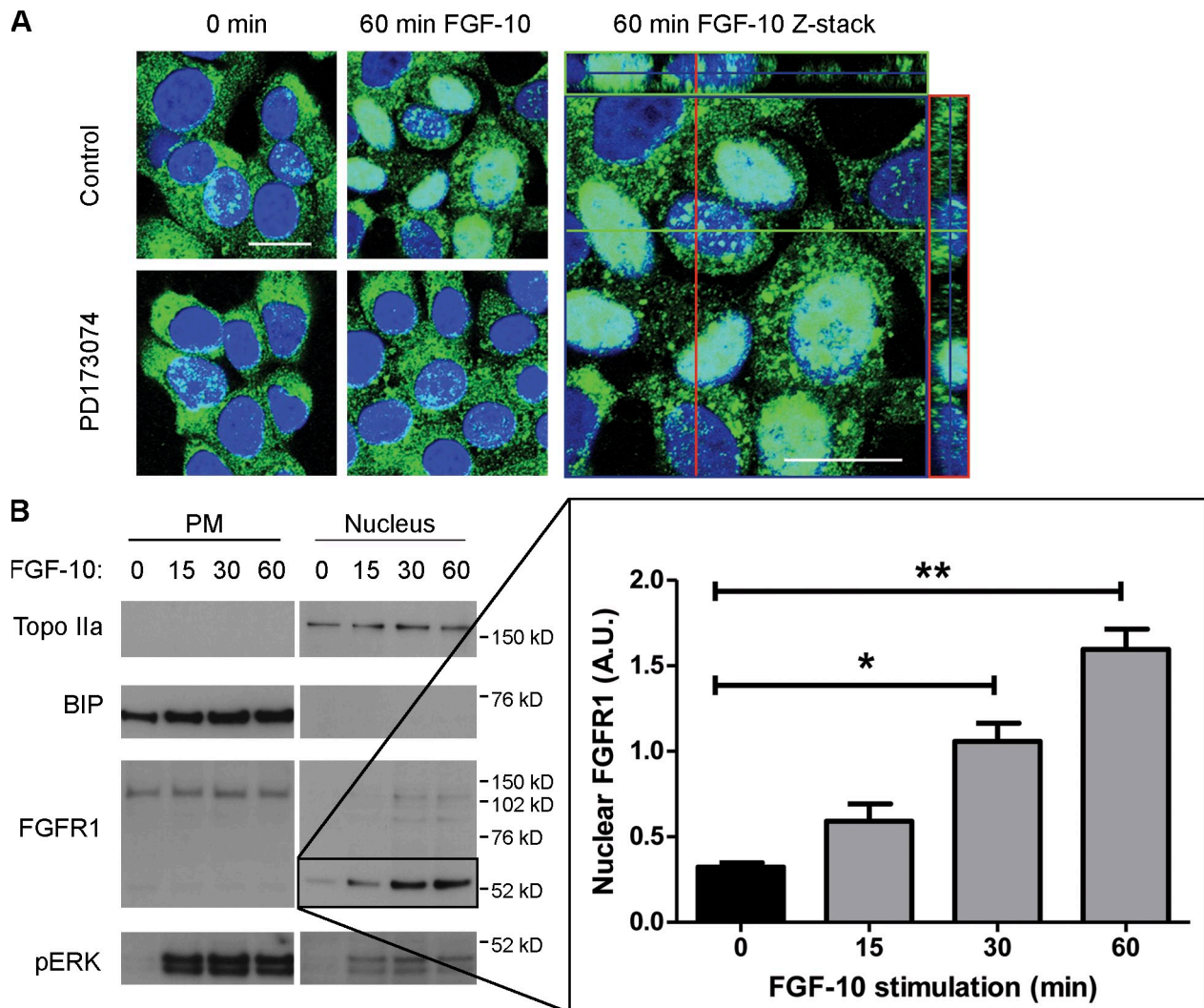
Figure 2. **Subcellular localization of FGFR1 in 2D culture.** (A) FGF-10 stimulation (60 min) resulted in increased nuclear FGFR1 localization in serum-starved MCF-7 cells, confirmed by examining confocal z-stack sections. The effect was abolished in the presence of PD173074. The green, purple, and red boxes represent the x-z and y-z scan perspectives from the confocal z stack. Bars, 25 µm. (B) Subcellular fractionation revealed that FGF-10 treatment increased nuclear FGFR1 localization in MCF-7 cells. Over a time course of FGF-10 stimulation (0–60 min), there was a significant increase in accumulation of a truncated 55-kD C-terminal fragment of FGFR1 in the nuclear fraction (highlighted in black box), but there was no change in full-length FGFR1 levels. Immunoblotting with anti-TOPOIIa and anti-BIP antibodies confirmed the specificity of the cell fractionation protocol, and pERK confirmed the efficiency of FGF-10 stimulation. Nuclear FGFR1 was normalized to the nuclear marker TOPOIIa, confirming the significance of the accumulation (graph; *, $P \leq 0.05$; **, $P \leq 0.01$ [Student's t test]). Error bars show means ± SEM. A.U., arbitrary unit; PM, plasma membrane.

(Fig. 4, A–C). MCF-7 cells growing in complete medium were treated with 25 and 50 µM GrB inhibitor for 6, 12, 24, and 48 h (Fig. S2 A). No change in nuclear FGFR1 localization was observed after 6 h of treatment. However, treatment with GrB inhibitor abolished nuclear FGFR1 after 24 h without changing the total FGFR1 protein levels (Fig. 4 C). The effect was apparent after 12 h of treatment and sustained up to ≥48 h (Fig. S2 A).

To confirm that GrB inhibition could block FGF-10–induced migration, we performed Transwell migration assays on MCF-7 cells in the presence or absence of GrB inhibitor and FGF-10 (Fig. 4 D). GrB inhibition completely and specifically blocked FGF-10–induced migration. Although inhibitor-treated cells clearly migrated less than control unstimulated cells, they still were capable of mounting a significant migratory response to EGF (Fig. 4 D). This effect also was observed when MCF-7 cells were treated with RNAi to GrB (Fig. S2, B and C).

To demonstrate direct GrB activity in MCF-7 cell lysates, we performed GrB activity assays using a chromogenic substrate, Ac-IEPD-pNA (Fig. 4, E and F; and Fig. S3). The efficacy of the assay was confirmed using human recombinant GrB as a positive control, with increasing concentrations of recombinant GrB producing increasing signals (Fig. S3 A). Furthermore, we confirmed the inhibition of recombinant GrB activity by 3,4-dichloroisocouramin (DCI; an inhibitor of serine proteases) upon inclusion of the inhibitor (50 µM) in the reaction mix (Fig. S3 B). Lysates from serum-starved MCF-7 cells treated for 1 h with FGF-10 showed significantly increased GrB activity, as measured hourly after incubation for 0–4 h with the chromogenic substrate Ac-IEPD-pNA (Fig. 4 E). Similarly, 15-min treatment with FGF-10 was sufficient to increase GrB activity but only after 3-h incubation with the Ac-IEPD-pNA substrate (Fig. S3 C). Importantly, pretreatment
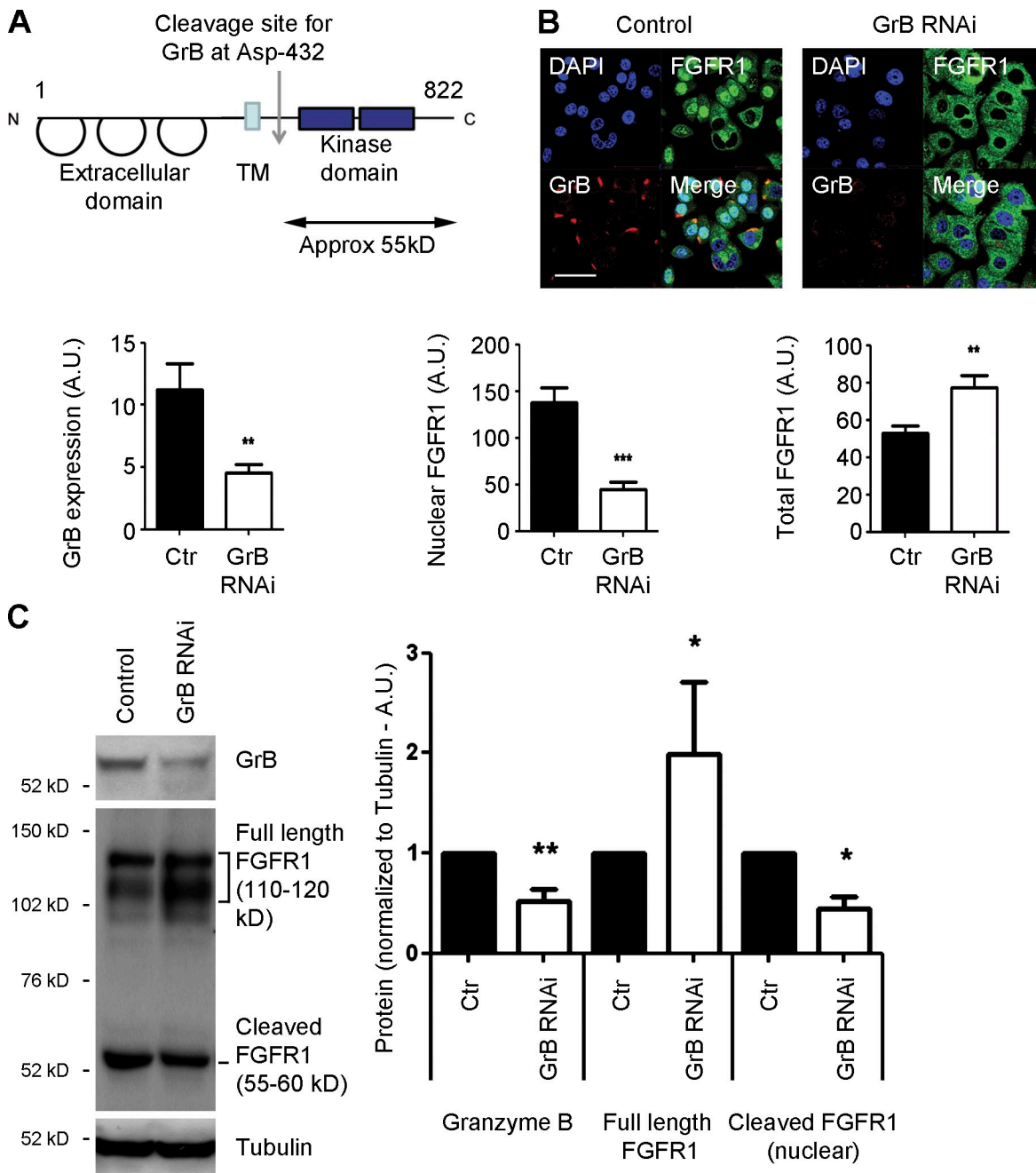
Figure 3. Inhibition of GrB by RNAi in MCF-7 cells reduced nuclear FGFR1 accumulation. (A) Schematic representation of FGFR1 depicting the three IgG loops of the extracellular domain, the transmembrane region (TM), and the split tyrosine kinase domain. The arrow indicates GrB cleavage site at Asp-432. Numbers indicate amino acid residues. Adapted from Loeb et al. (2006). N, N terminus; C, C terminus. (B) Treatment of MCF-7 cells, growing in serum-containing medium, with a GrB inhibitor abolished nuclear FGFR1 after 24 h but did not change the total FGFR1 protein levels. Confocal analysis of MCF-7 cells growing in serum-containing medium treated with GrB RNAi for 72 h revealed efficient knockdown of GrB concomitant with decreased nuclear FGFR1 staining. **, P < 0.01; ***, P < 0.001 (Student's t test). Bar, 25 µm. (C) Western blot analysis confirmed that GrB was expressed in MCF-7 cells and showed that 72-h treatment with RNAi to GrB reduced levels of nuclear FGFR1, despite an overall increase in full-length FGFR1. *, P < 0.05; **, P < 0.01 (Mann–Whitney test). Error bars show means ± SEM. A.U., arbitrary unit; Ctr, control.

with DCI before FGF-10 treatment blocked the induction of GrB activity (Fig. 4 E). Furthermore, 50 µM DCI treatment (5 h) of MCF-7 cells growing in complete medium resulted in a significant decrease in both GrB activity (Fig. 4 F) and in cleaved nuclear FGFR1 protein (Fig. 4 G).

The mechanism of FGFR1 cleavage by GrB was investigated by mutating the GrB cleavage site within FGFR1b as described previously (Fig. 5 A; Loeb et al., 2006). Confocal

analysis revealed that, 48 h after transient transfection, MCF-7 cells with wild-type (WT) FGFR1b (VSAD) expressed high levels of both full-length and nuclear FGFR1 compared with empty vector–transfected control cells. Cells transfected with mutant FGFR1b (VSAN) expressed higher levels of full-length FGFR1 compared with control-transfected cells (pcDNA4/TO) but did not show high levels of nuclear FGFR1 (Fig. 5 B). The functional relevance of this finding was tested using Transwell
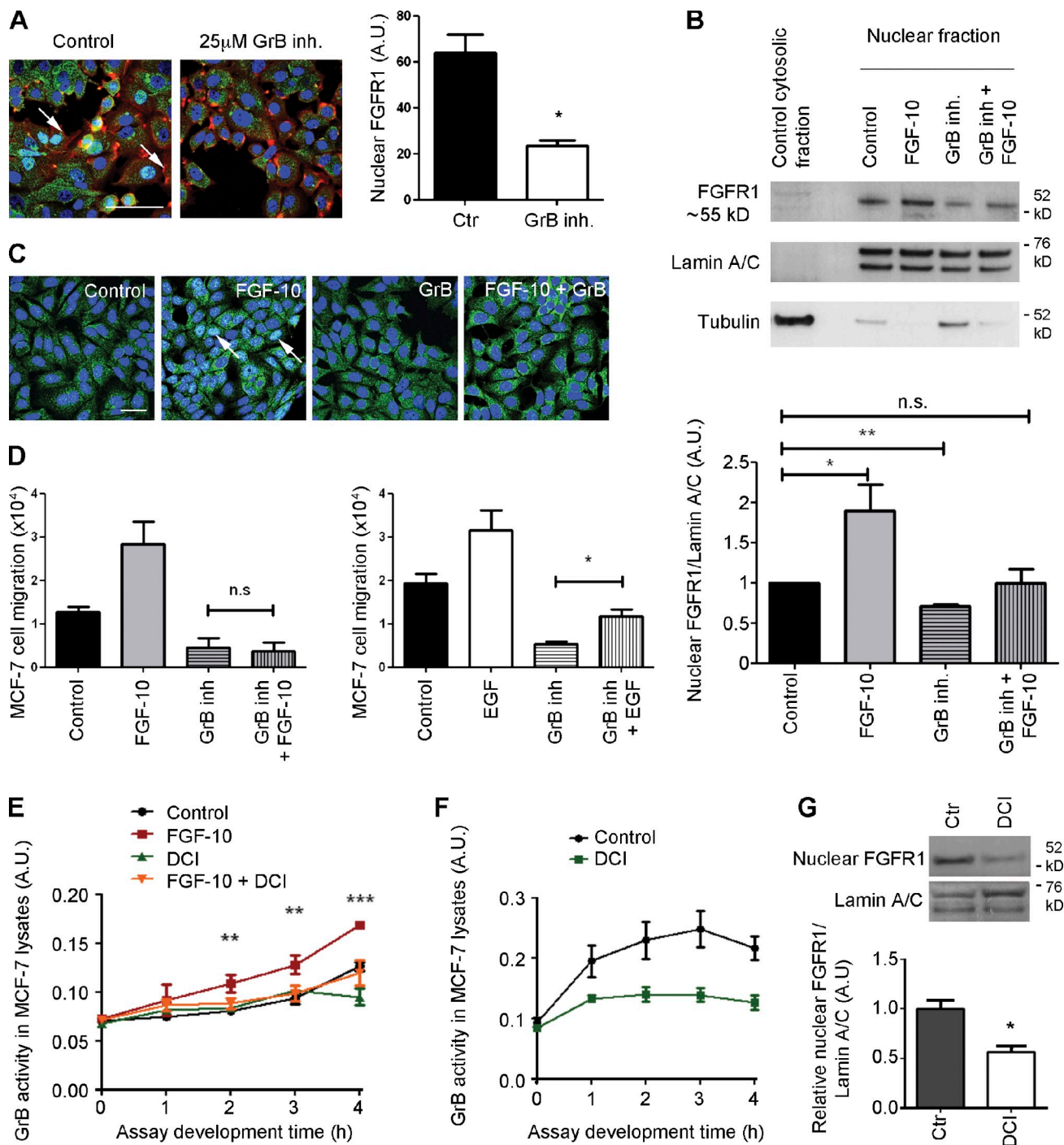
Figure 4. **Treatment of MCF-7 cells with a GrB inhibitor reduced nuclear FGFR1 accumulation and blocked FGF-10–dependent cell migration.** (A) Treatment of MCF-7 cells, growing in serum-containing medium, with a GrB inhibitor (inh.) abolished nuclear FGFR1 (arrows) after 24 h but did not change the total FGFR1 protein levels. *, P < 0.05 (ANOVA). Bar, 100 µm. (B) Subcellular fractionation confirmed that FGF-10 treatment (1–2 h) increased nuclear FGFR1 (a truncated 55-kD C-terminal fragment of FGFR1) in serum-starved MCF-7 cells and decreased it when cells were treated with 25 µM GrB inhibitor (24 h). When cells were pretreated with GrB inhibitor and then treated with FGF-10, the translocation of the nuclear FGFR1 was partially blocked. Immunoblotting with Lamin A/C and tubulin antibodies confirmed the specificity of the cell fractionation protocol. Nuclear FGFR1 was normalized to the nuclear marker Lamin A/C, confirming the significance of the accumulation (graph). (C) MCF-7 cells were treated with 25 µM GrB inhibitor (24 h) in serum-free medium before stimulation with FGF-10/heparin (100 ng/ml and 7.5 µg/ml, respectively). Control cells showed increased staining for nuclear FGFR1 (arrows) after FGF-10 treatment, and this was blocked by GrB inhibition. Bar, 25 µm. (D) Transwell migration assays with MCF-7 cells showed that GrB inhibition abolished the promigratory effect of FGF-10. In contrast, cells were still able to migrate in response to EGF stimulation. *, P ≤ 0.05; **, P ≤ 0.01 (Student's t test). (E) GrB activity in lysates from serum-starved MCF-7 cells with or without FGF-10/heparin treatment (100 ng/ml and 7.5 µg/ml, respectively) in the presence or absence of pretreatment with the serine protease inhibitor 3,4-dichloroisocoumarin (DCI; 50 µM; 1-h pretreatment). Activity was measured at 405-nm absorbance at hourly intervals after the addition of 200 µM Ac-IEPD-pNA substrate. FGF-10 treatment significantly increased GrB activity in MCF-7 cells, but this effect was abrogated by pretreatment with DCI. **, P ≤ 0.01; ***, P ≤ 0.001 (Student's t test). (F) GrB activity in MCF-7 cells growing in full serum is markedly reduced by treatment with 50 µM DCI (2 h). (G) 5-h treatment with 50 µM DCI decreased nuclear FGFR1 protein significantly. *, P ≤ 0.05 (Student's t test). Error bars show means ± SEM. A.U., arbitrary unit; Ctr, control.

A

WT FGFR1b (VSA**D**)   V S A **D**

gtg tct gct **g**ac

Mutant FGFR1b (VSA**N**)   gtg tct gct **a**ac
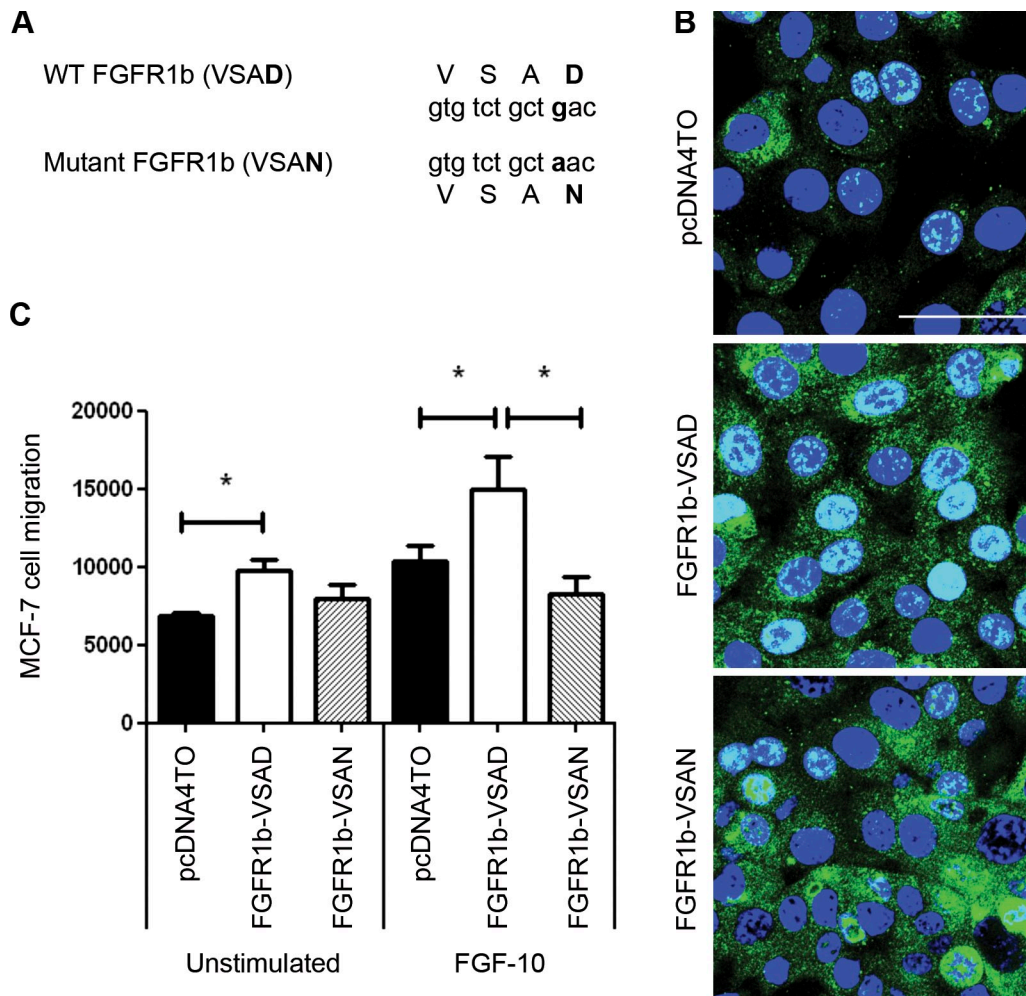
V S A **N**

B

C

Figure 5. **Mutation of GrB cleavage site inhibited nuclear translocation of FGFR1.** (A) Site-directed mutagenesis on wild-type (WT) FGFR1 changed the guanine nucleotide at position 1963 to adenine (**g**1963**a**; using sequence available from GenBank/EMBL/DDBJ under accession no. NM_023106.2) and thereby amino acid 432 from aspartic acid to alanine (**D**432**N**), abolishing the GrB cleavage site in Mutant FGFR1. (B) Confocal analysis of MCF-7 cells transiently transfected (48 h) with WT (VSAD) or mutant (VSAN) FGFR1b revealed that mutant (VSAN) FGFR1b did not translocate to the nucleus. Bar, 50 µm. (C) Transwell migration assays showed that, under control conditions, MCF-7 cells transfected with WT FGFR1b (VSAD) migrated more compared with empty vector (pcDNA4/TO)– and mutant FGFR1b (VSAN)–transfected cells. FGF-10 stimulation increased migration in cells transfected with WT FGFR1b (VSAD) but did not affect MCF-7 cells transfected with mutant FGFR1b (VSAN). *, P ≤ 0.05 (paired Student's t test and ANOVA). Error bars show means ± SEM.

migration assays (Fig. 5 C). Under control conditions (unstimulated cells), MCF-7 cells transfected with WT FGFR1b (VSAD) migrated significantly more than empty vector (pcDNA4/TO)– or mutant FGFR1b (VSAN)–transfected cells. Importantly, FGF-10 stimulation increased cell migration in MCF-7 cells transfected with WT FGFR1b (VSAD) or empty vector (pcDNA4/TO) but did not have an effect on MCF-7 cells transfected with mutant FGFR1b (VSAN).

To investigate further the potential role of the cleaved intracellular fragment (IC) of FGFR1, we cloned the cDNA encoding the C-terminal cleaved portion into an expression vector, pcDNA4/TO, adding a C-terminal MYC epitope tag (Fig. 6 A). Efficient expression of the construct after transient transfection into MCF-7 cells was determined by Western blotting and immunofluorescence (Fig. 6 A). Expression either of full-length FGFR1 or IC-FGFR1-MYC in MCF-7 cells resulted in significantly increased Transwell migration
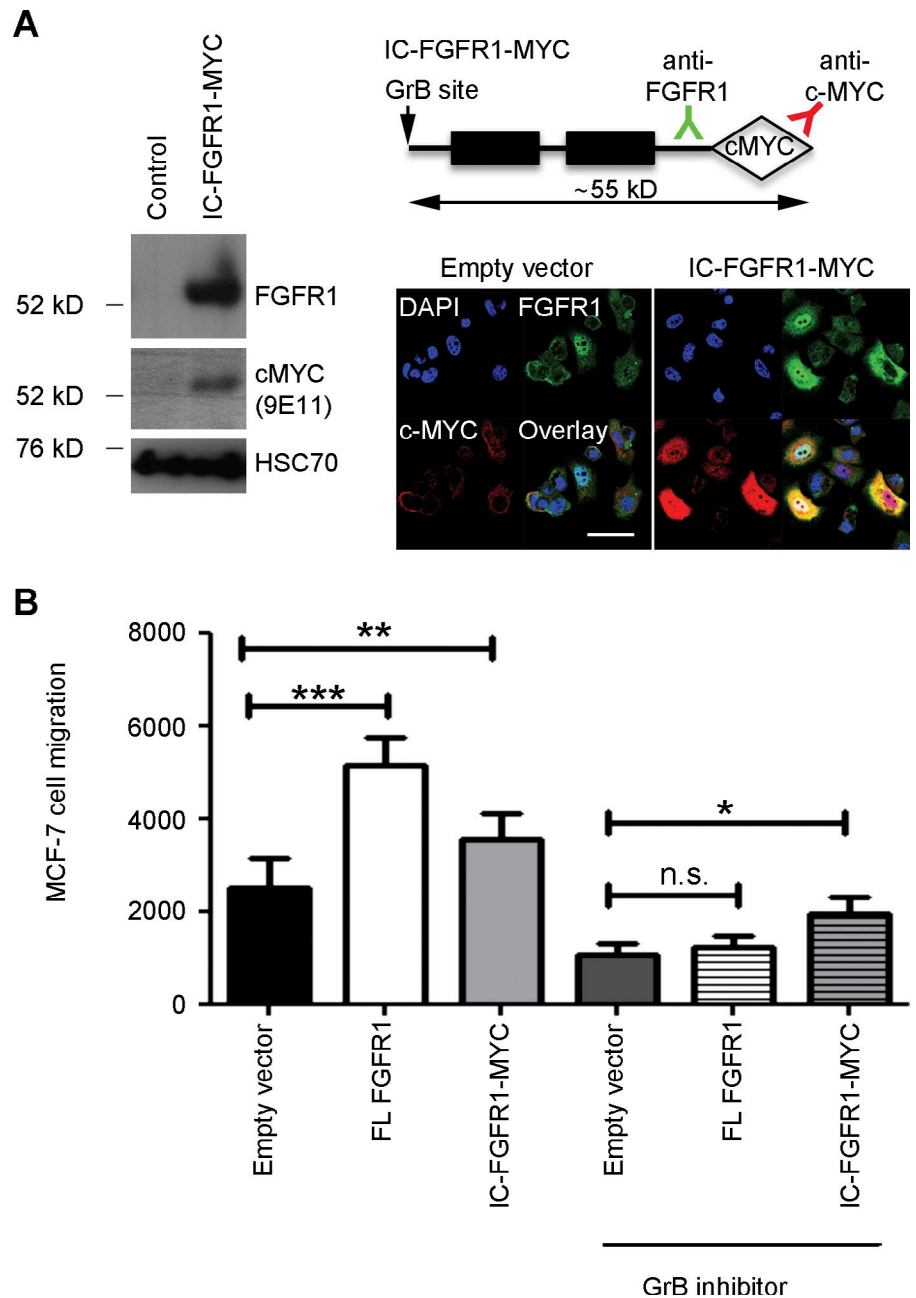
compared with empty vector–transfected control cells. However, in the presence of GrB inhibitor, the promigratory effect of the full-length receptor was abrogated, whereas cells expressing IC-FGFR1-MYC still showed significantly enhanced migration (Fig. 6 B).

How GrB is activated after FGF-10 stimulation is the subject of ongoing experiments in the laboratory. Initial observations revealed that, immediately after FGF-10 stimulation of serum-starved MCF-7 cells, there was a clear increase in expression and processing of Cathepsin C (Fig. S4 A), concomitant with an increase in GrB protein levels.

Nuclear localization of FGFR1 in 3D culture and in vivo

Because FGFR1 localized to the nucleus specifically in breast cancer cells stimulated with FGF-10, we used an organotypic model to investigate the phenomenon in a more physiological

Figure 6. **Expression of the intracellular domain of FGFR1 in MCF-7 cells increased cell migration and bypassed GrB inhibition.** (A) Western blotting confirmed successful transfection of the intracellular C-terminal FGFR1 (IC-FGFR1-MYC) fragment in MCF-7 cells. A 55-kD band was present with both anti-FGFR1 antibody or an anti–c-MYC antibody. Similarly, immunofluorescence showed enhanced nuclear FGFR1 in the cells transfected with the IC-FGFR1-MYC construct. Bar, 25 µm. (B) Transwell migration assays showed that, under control conditions, MCF-7 cells transfected with both full-length FGFR1b and IC-FGFR1-MYC migrated more compared with empty vector (pcDNA4/TO) cells. GrB inhibition decreased migration in all cells transfected with empty vector, full-length (FL) FGFR1b, or IC-FGFR1-MYC compared with untreated cells, but there was a significant difference in the cells transfected with IC-FGFR1-MYC compared with empty vector, whether or not there was no difference between cell transfected with full-length FGFR1b. *, $P \leq 0.05$; **, $P < 0.01$; ***, $P < 0.001$ (paired Student's t test and ANOVA). Error bars show means ± SEM.

microenvironment. The organotypic culture (OC) consisted of a collagen/Matrigel mix containing human foreskin fibroblasts, as the stromal equivalent, overlaid with MDA-MB-231 cells (Fig. 7 A; Chioni and Grose, 2008). The OC was raised to an air–liquid interface and cultured for 10 d before fixation. Hematoxylin and eosin staining revealed invading particles (group of cells) within the stroma (Fig. 7 B). Staining of the OC with anti–FGF-10 and anti-FGFR1 antibodies showed that FGF-10 was expressed highly both in invading and noninvading cells (Fig. 7 C). However, FGFR1 was localized mainly to the nucleus in invading cells, whereas in the noninvading cells, it was mainly in the plasma membrane and cytoplasm (Fig. 7 C). Still images and videos obtained by optical projection tomography on OCs stained with the neonatal voltage-gated sodium channel (NESO) antibody (a marker for metastatic breast cancer cells;

Chioni et al., 2005) showed that the invading cells formed distinct groups within the stroma (Fig. 7 D and Video 1). Ki67 staining of transverse sections from the OC revealed that cell proliferation was restricted to invading cells and not those cells that have remained at the air–liquid interface (Fig. 7 E). A breast cancer OC growing for 10 d in the presence of the PD173074 inhibitor showed significantly less cancer cell invasion compared with controls, as judged by quantification of their invasion index (Fig. 7, F and G). Immunohistochemical and immunofluorescent staining of tissues from breast cancer patients with an anti-FGFR1 antibody revealed specific FGFR1 staining in the myoepithelial compartment of ductal carcinoma in situ, and even stronger staining was detected in invasive carcinoma, including nuclear staining in some invading cells (Fig. 7, H and I).
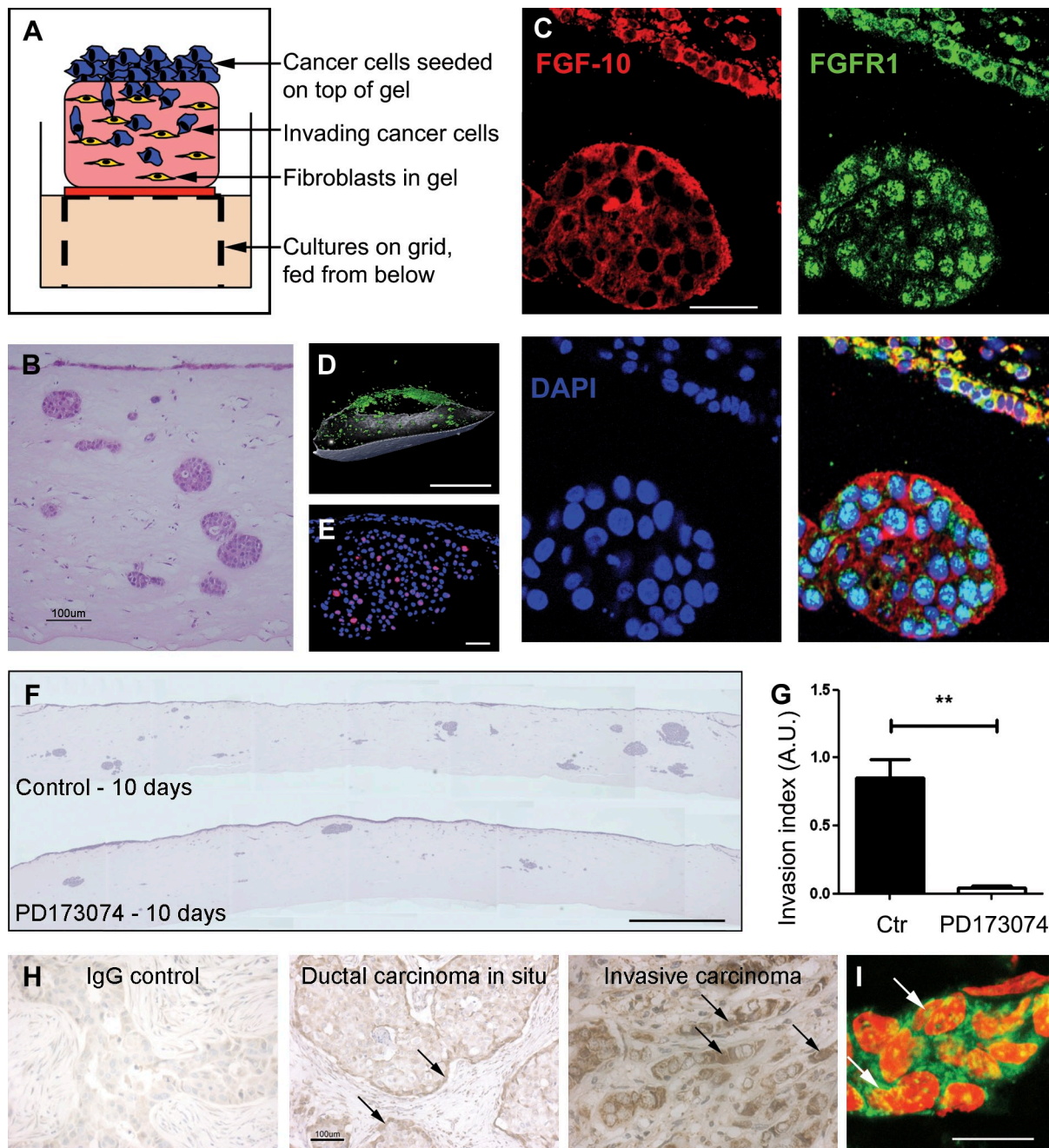
Figure 7. **FGFR1 localizes to the nucleus in invading cells in 3D culture and in vivo.** (A) A breast cancer organotypic model was designed using a collagen/Matrigel mix containing human foreskin fibroblasts as the stromal equivalent, overlaid with MDA-MB-231 cells. OCs were raised into an air–liquid interface and cultured for 10 d before fixation in 4% PFA. (B) Hematoxylin and eosin staining revealed invading particles (group of cells) in the stroma. (C) FGF-10 was highly expressed in both invading and noninvading cells. FGFR1 was localized mainly to the nucleus (DAPI stain) of invading cells and remained mainly in the plasma membrane and cytoplasm of noninvading cells. (D) Still optical projection tomography image of an OC stained with NESO antibody, a marker for metastatic breast cancer cells (Chioni et al., 2005), highlighted that the invading cells formed distinct groups within the stroma (Video 1). (E) Anti-Ki67 staining of transverse sections from OCs revealed that cell proliferation was restricted to invading cells and not those cells that remained at the air–liquid interface. (F and G) Breast cancer OCs growing for 10 d in the presence of PD173074 showed significantly less cancer cell invasion compared with control. The invasion index comprises the combined measurements of (a) depth of invasion (mean of several measurements from each OC, taken from the top layer of the noninvading cells to the middle of the invading particles). (b) number of invading particles, and (c) mean area of the invading particles (n = 4 OCs for each condition). Error bars show means ± SEM. (H) Immunohistochemistry of human tissues from patients with an anti-FGFR1 antibody revealed that, although the IgG negative control remained clear for brown DAB staining (left), specific FGFR1 staining was detected in the myoepithelial compartment of ductal carcinoma in situ (arrows in middle image) and even stronger staining was detected in invasive lobular carcinoma (arrows in right image), including nuclear staining in some invading cells (B). This is shown by confocal sectioning of immunofluorescently stained invasive carcinoma, in which FGFR1 (green) can be seen in the nuclei (red) as labeled by open arrows (colocalization in yellow). **, P ≤ 0.01 (ANOVA). Bars: (B, F, and H) 100 µm; (C, E, and I) 50 µm; (D) 500 µm.

Table 1. **Regulation of FGFR1 target genes**

Gene	FGFR1b-VSAD		FGFR1 RNAi		FGFR1b-VSAN	
	Fold change	P-value	Fold change	P-value	Fold change	P-value
EBI3	0.25 ± 0.02	<0.001	1.93 ± 0.26	<0.05	1.07 ± 0.39	NS
GRINA	0.7 ± 0.14	<0.05	7.38 ± 5.5	NS	1.55 ± 0.57	NS
KRTAP5-6	4.25 ± 1.66	NS	0.27 ± 0.05	<0.01	0.77 ± 0.27	NS
POU2F2	2.42 ± 1.3	NS	1.34 ± 0.35	NS	–	–
PRSS27	3.25 ± 1.6	NS	0.31 ± 0.05	<0.01	1.53 ± 0.63	NS
SFN	3.76 ± 1.56	<0.05	0.57 ± 0.11	<0.05	1.17 ± 0.26	NS
STAC3	0.75 ± 0.13	<0.05	0.5 ± 0.12	<0.01	–	–

Fold change of mRNA expression in MCF-7 cells of genes identified after ChIP on chip with an anti-FGFR1 antibody, after 48-h overexpression of WT (VSAD) FGFR1b, 48-h RNAi of FGFR1, or 48-h overexpression of GrB-resistant (VSAN) FGFR1b. Real-time PCR was analyzed using the $2^{-\Delta\Delta Ct}$ method and using expression of HPRT and GAPDH as housekeeping genes for normalization. Data presented in the table are normalized with GAPDH. $n \geq 3$ independent experiments in triplicate. Minus signs indicate where analysis was not performed. Statistical significance was tested with both Mann–Whitney and Student's t test.

Nuclear FGFR1 is involved in transcriptional regulation of target genes

Eight potential FGFR1 target genes were determined by chromatin immunoprecipitation (ChIP) on chip analysis of MCF-7 cells using an anti-FGFR1 antibody (Fig. S4 B). Each gene was present in at least three of eight FGFR1 ChIP on chip datasets and not present in any of five IgG controls. Whole-cell extracts, as well as samples immunoprecipitated with RNA polymerase II antibody, were used as positive controls. Because *MARK3* was not amplified in our repeat samples, we did not investigate it further. *STAC3* showed strong amplification, so despite one of the five IgG samples showing putative binding, we decided to continue studying it. Primers for the promoter region of *glyceraldehyde 3-phosphate dehydrogenase* (*GAPDH*) were used as a negative control for the samples immunoprecipitated with FGFR1 and IgG because it was not present as a putative target in any of our ChIP on chip datasets (Fig. S4 B).

Putative FGFR1 target genes identified by ChIP on chip were analyzed by real-time RT-PCR expression analysis after RNAi-mediated FGFR1 knockdown (Fig. S1) or transient overexpression of FGFR1b (Fig. S5, A–C). FGFR1b overexpression was confirmed by real-time RT-PCR (Fig. S5 A) and by immunofluorescence using an anti-FGFR1 antibody (Fig. S5 B). Western blotting with an anti-FGFR1 antibody also showed a significant increase in FGFR1 protein (Fig. S5 C). Both full-length FGFR1 and cleaved FGFR1 were up-regulated 48 h after transfection (sixfold and 2.5-fold increase, respectively; Fig. S5 C).

Table 1 shows changes in target gene mRNA expression in MCF-7 cells after FGFR1b overexpression or FGFR1 knockdown (both at 48 h). Data presented are normalized to GAPDH, with hypoxanthine-guanine phosphoribosyltransferase (HPRT) normalization giving identical results (unpublished data). Although levels of POU2F2 expression tended to increase upon either up- or down-regulation of FGFR1 expression, STAC3 behaved in the opposite fashion, so these were not investigated further. However, FGFR1 acted clearly as a transcriptional repressor for EBI3 and GRINA, whereas it activated expression of KRTAP5-6 (Keratin-associated protein 5-6), PRSS27 (also called Marapsin), and Stratifin (SFN).

Furthermore, RNAi-mediated knockdown of GrB led to up- and down-regulation of negatively and positively regulated FGFR1 target genes, respectively (Fig. 8). Transient overexpression of IC-FGFR1 resulted in increased expression of KRTAP5-6 and PRSS27, though not all target genes showed significant changes in expression in these transient transfections. Expression of GrB-resistant FGFR1b VSAN did not affect target gene expression (Table 1).

To confirm that these FGFR1-regulated genes could control cell behavior, we performed individual RNAi-mediated knockdown of each of the targets in MCF-7 cells and assessed the subsequent impact on cell migration. All of the target genes showed efficient knockdown of expression at 48 h after RNAi transfection (Fig. 8 A), and where the antibody was available in house, we also confirmed knockdown at the protein level (Fig. 8 A*). Cells in which target gene expression had been knocked down were used subsequently in Transwell migration assays (Fig. 8 B). Knockdown of mRNA for each of the target genes up-regulated by FGFR1 (*KRTAP5-6*, *SFN*, and *PRSS27*) resulted in significantly decreased MCF-7 cell migration, whereas migration was increased after knockdown of mRNA for the target genes down-regulated by FGFR1 (*GRINA* and *EBI3*). The reduction in migration after KRTAP5-6, SFN, and PRSS27 knockdown was identical to that seen when FGFR1 was targeted, and compound knockdown of all three FGFR1 up-regulated targets, with or without concomitant knockdown of FGFR1, produced no further reduction in cell migration (Fig. 8 B).

Discussion

FGFR signaling plays critical roles during embryogenesis and, in the adult, regulating a wide range of cell behaviors, including proliferation, migration, survival, and differentiation. Such a mechanism is highly susceptible to hijacking by cancer cells seeking to gain a growth advantage. Indeed, the link between aberrant FGFR signaling and developmental abnormalities and tumorigenesis is unequivocal (Turner and Grose, 2010). Amplifications of both *FGFR1* and *FGFR2* are reported in ≤10% of breast cancer patients, and at least for *FGFR1*, amplification is associated with a poorer outcome (Reis-Filho et al., 2006; Elbauomy Elsheikh et al., 2007). In particular, amplification and subsequent overexpression of FGFR1 contributes to poor prognosis in luminal-type breast cancers, driving endocrine
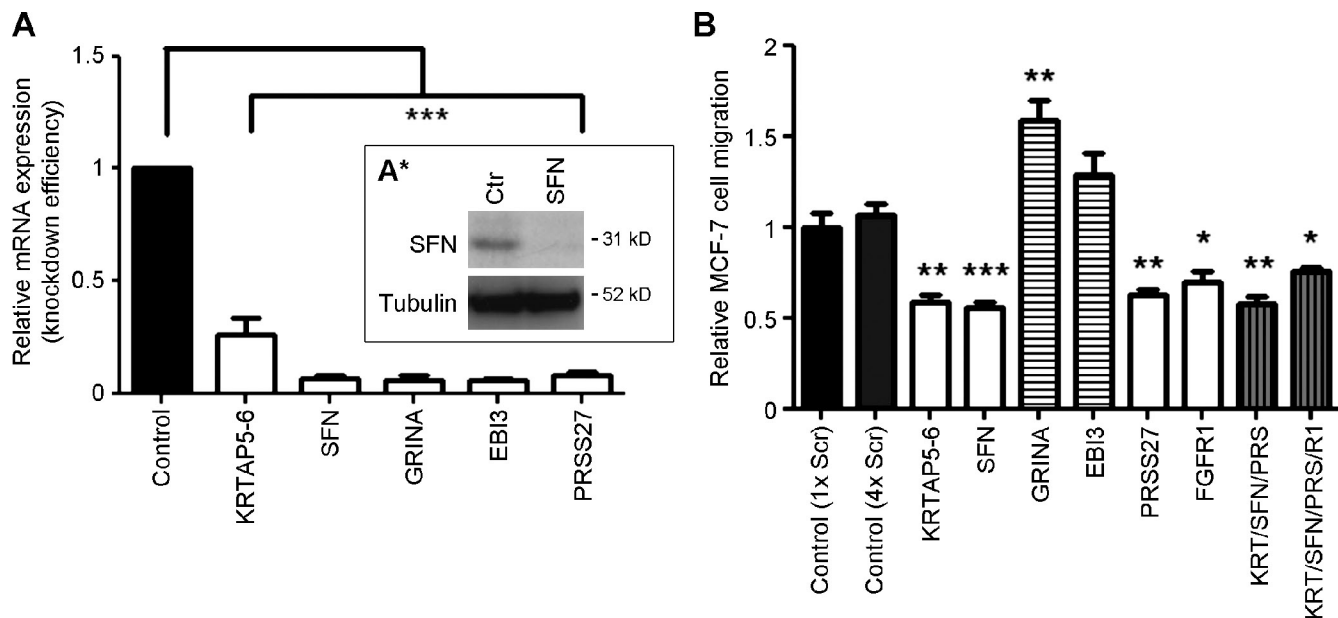
Figure 8. **Down-regulation of FGFR1 target genes by RNAi had an effect on cell migration.** (A and B) Transwell migration assay showed that after 48-h RNAi treatment of KRTAP5-6, Stratifin (SFN), and PRSS27, MCF-7 cells migrated less compared with control cells (scrambled [Scr] RNAi treated). However, 48-h RNAi treatment of GRINA and EBI3 genes increased cell migration. *, $P \leq 0.05$; **, $P < 0.01$; ***, $P < 0.001$ (paired Student's *t* test). Error bars show means ± SEM. Ctr, control; KRT, keratin; PRS, PRSS27.

therapy resistance (Turner et al., 2010). Indeed, *FGFR1* amplification is the strongest independent predictor of poor outcome in patients with ER-positive tumors (Elbauomy Elsheikh et al., 2007). However, despite many studies, the mechanism by which FGFR signaling might control metastatic cell behavior and contribute to cancer progression is far from clear. Our study identifies a novel mechanism by which FGFR1 signaling regulates cancer cell behavior.

Upon ligand binding, FGFRs are known to activate several downstream signaling pathways, including PI3K, PLC-γ, and MAPK (Ornitz and Itoh, 2001). We focused on the ER-positive MCF-7 breast cancer cell line, which activates the MAPK signaling pathway rapidly upon FGF-10 stimulation. As expected, this was abrogated by pretreatment with a specific inhibitor for FGFR (PD173074; Fig. 1 A; Mohammadi et al., 1998).

Having confirmed that FGFR signaling was eliciting the anticipated functional effects in cells, we focused specifically on FGFR1, investigating the subcellular trafficking of the receptor after ligand binding. Using recombinant FGF-10 as a known ligand of FGFR1b (Zhang et al., 2006), we observed a dramatic localization of FGFR1 to the nucleus after receptor activation (Fig. 2 A and Fig. S1) and showed that a 55–60-kD C-terminal portion of the receptor accumulated in the nucleus (Fig. 2 B).

Several studies have reported nuclear localization of full-length FGFRs (Maher, 1996; Stachowiak et al., 1996a,b; Reilly and Maher, 2001; Zammit et al., 2001; Peng et al., 2002; Myers et al., 2003; Reilly et al., 2004; Dunham-Ems et al., 2009), but in contrast to other RTKs (Carpenter and Liao, 2009), there has been no evidence in the literature for receptor cleavage being implicated in nuclear translocation. Cleavage of FGFR1 has been reported previously (Levi et al., 1996; Hanneken, 2001;

Loeb et al., 2006) but not in the context of nuclear trafficking. First described as a target for MMP-2 (Levi et al., 1996), the focus was on the proteolytic shedding of FGFR1 and its potential functional effects (Hanneken, 2001) rather than what happened to the intracellular portion of the receptor. A later study identified FGFR1 as a substrate for the serine protease GrB, but the context again was different, with cleavage of FGFR1 thought to prevent survival signaling caused by cleavage between the ligand binding and tyrosine kinase domains (Loeb et al., 2006). Most interestingly, this latter study reported that cleavage by GrB generated a 55–60-kD C-terminal receptor fragment. The cleavage site for GrB is unique to FGFR1 among the FGFRs.

Having determined that our breast cancer cell lines expressed GrB, we investigated whether endogenous GrB was mediating cleavage of FGFR1 in a fashion similar to the way that exogenous GrB was shown to cleave FGFR1 in prostate cancer cells (Loeb et al., 2006). Treatment with a GrB synthetic peptide inhibitor (Martin et al., 1998), a serine protease inhibitor, DCI (Harper et al., 1985), or with RNAi to GrB led to significant reductions in FGFR1 nuclear localization (Fig. 3 and Fig. 4), suggesting that GrB indeed plays an important role in the process. Treatment with the GrB inhibitor increased levels of full-length FGFR1 (Fig. 3 C), indicating that GrB might be involved in receptor turnover. Importantly, inhibition of GrB blocked accumulation of nuclear FGFR1 after FGF-10 treatment (Fig. 4, B and C) and, at a functional level, blocked the promigratory effect of FGF-10 treatment (Fig. 4 D and Fig. S2, B and C). These data suggested that activation of the classical FGFR1 signaling cascade alone was not sufficient to drive cell migration but that nuclear localization of the receptor may also be critical. The effect of GrB inhibition clearly did not affect solely FGFR1 because the inhibition of baseline migration in unstimulated cells was impaired significantly when cells were

treated with GrB inhibitor (Fig. 4 D) compared with the specific FGFR inhibitor PD173074 (Fig. 1 B). Indeed, the peptide inhibitor is known to also inhibit Caspase 8 (Thornberry et al., 1997). However, cells treated with GrB inhibitor were still capable of mounting a significant migratory response after treatment with EGF, a known motogenic stimulus (Xie et al., 1995). Critically, this confirmed that the antimigratory effect of GrB inhibition was not simply the result of a catastrophic effect on cell viability.

Further evidence that GrB activity was induced in serum-starved MCF-7 cells upon FGF-10 treatment was provided by in vitro GrB activity assay. The significant increase in GrB activity seen after FGF-10 stimulation was blocked completely by treatment with the serine protease inhibitor DCI (Fig. 4 E). Indeed, MCF-7 cells growing in complete medium showed significant GrB activity that was blocked by treatment with DCI (Fig. 4 F). Because DCI treatment blocks granzyme but not caspase activity, these data suggest that, in our activity assay, substrate cleavage was dependent on the serine protease GrB and not affected by Caspase 8, which can cleave the Ac-IEPD-pNA substrate (Thornberry et al., 1997). Together with the findings that either DCI treatment (Fig. 4 G) or RNAi-mediated knockdown of GrB (Fig. 3) decreased levels of cleaved nuclear FGFR1, our data strongly support the hypothesis that FGF-10 treatment increases nuclear FGFR1 via GrB-mediated cleavage (Fig. 2 and Fig. 4, B and G).

Interestingly, an antibody recognizing a juxtamembrane region of FGFR1, N terminal to the GrB cleavage site, also showed positive FGFR1 nuclear staining, suggesting that the N-terminal fragment of the receptor also enters the nucleus. Unfortunately, the antibody did not work on Western blots, so this could not be confirmed by cell fractionation, but the lack of full-length FGFR1 in the nuclear fraction, seen when we blotted with our C-terminal antibody, suggested that the N-terminal staining must represent a cleaved portion of the receptor.

To confirm the significance of GrB-mediated cleavage of FGFR1, we mutated the GrB cleavage site of the full-length human FGFR1b (Fig. 5 A) as described previously (Loeb et al., 2006). Immunofluorescent staining for FGFR1 revealed that MCF-7 cells transfected either with WT or cleavage-resistant full-length FGFR1 expressed high levels of FGFR1 protein (Fig. 5 B). However, although the WT receptor was seen clearly in the nucleus, cells transfected with the mutant receptor showed no more nuclear FGFR1 than empty vector–transfected cells. When the functional significance of this finding was tested by assaying migration in the presence or absence of FGF-10, cells transfected with WT FGFR1 showed a significant increase in migration both in unstimulated and stimulated conditions, when compared with control cells (Fig. 5 B). In contrast, cells transfected with mutant FGFR1 showed no increase in their migratory capacity, indicating that cleavage and nuclear trafficking of FGFR1 is critical to its promigratory effect. These data were reinforced by the finding that cells transfected with a construct expressing the cleaved intracellular portion of FGFR1 showed enhanced migratory potential, even in the presence of a GrB inhibitor. In contrast, cells expressing a full-length FGFR1 construct displayed enhanced migration under normal culture

conditions, but this effect was blocked completely when cleavage of the receptor was prevented by GrB inhibition (Fig. 6).

Having confirmed that nuclear localization of FGFR1 was critical for migration of breast cancer cells in 2D culture, we determined the expression pattern of FGFR1 in a more physiological 3D model (Fig. 7). FGFR1 was localized to the nucleus specifically in breast cancer cells that invaded into the stroma, and this invasion was impaired significantly by blocking FGFR signaling. Most interestingly, when we analyzed expression of FGFR1 in samples of human invasive breast cancer, we saw clear nuclear localization of FGFR1 in invading cells (Fig. 7, H and I). Nuclear localization of RTKs has been implicated in poor prognosis in a variety of studies (Zammit et al., 2001; Adam et al., 2003; Lo et al., 2005b; Li et al., 2009a; Xia et al., 2009). Collectively, our findings suggest that localization of FGFR1 to the nucleus may be critical to cell migration and invasion.

There is strong evidence that RTKs can act to regulate transcription of target genes in the nucleus (Xie and Hung, 1994; Lin et al., 2001; Wang et al., 2004; Lo et al., 2005a) and increasing data supporting a possible regulatory role for FGFR1 (Peng et al., 2002; Hu et al., 2004; Fang et al., 2005; Dunham-Ems et al., 2009). We identified several putative target genes for nuclear FGFR1 (Fig. S4 B and Table 1), the detailed study of which is the subject of ongoing studies. Of the three genes identified as being positively regulated by FGFR1, all have potential links with invasive cell behavior. PRSS27 is overexpressed in pancreatic cancer (Badea et al., 2008) as well as in hyperproliferative keratinocytes (Li et al., 2009b), SFN has been implicated in malignant lung cancer (Shiba-Ishii et al., 2011), and although the function of KRTAP5-6 is unknown, Keratin 6 is well documented as a marker of proliferative and migratory keratinocytes (Navarro et al., 1995). Less is known about a possible role in cancer for the two genes that were negatively regulated by FGFR1, *EBI3* (Devergne et al., 1996) and *GRINA* (Kumar et al., 1991). However, our ChIP data, together with modulation of FGFR1 levels in MCF-7 cells, either through overexpression or RNAi-mediated knockdown of the receptor coupled with GrB inhibition, showed that FGFR1 has a clear potential to regulate transcription of target genes, either directly or as part of a larger complex.

The functional relevance of these target genes was confirmed by RNAi-mediated knockdown experiments. All three genes identified as targets for up-regulation by FGFR1, *KRTAP5-6*, *SFN*, and *PRSS27*, were found to regulate MCF-7 cell migration positively. Conversely, targets that were negatively regulated by FGFR1, *GRINA* and *EBI3*, were found to inhibit cell migration (Fig. 8 B). Collectively, these observations support the hypothesis that nuclear FGFR1 might regulate an invasive gene expression signature. Interestingly, compound knockdown of all the promigratory target genes resulted in no additive impairment of migration, suggesting that the genes might lie in the same pathway.

Although studies of GrB function focus largely on cytotoxic lymphocytes and its induction of apoptosis in target cells, GrB expression has been observed in a range of cell types, including urothelial cancer cells (D'Eliseo et al., 2010)

and breast cancer cells (Hu et al., 2003). Notably, in urothelial cancer, expression of GrB was concentrated at the cancer invasion front (D'Eliseo et al., 2010). There is evidence that GrB plays a role in extracellular proteolysis (Buzza et al., 2005), though the literature is divided as to whether this activity is pro- or antiinvasive. Our data show clearly that endogenous GrB can play a promigratory role, at least in part through cleaving FGFR1.

Further studies into determining where in the cell receptor cleavage occurs are ongoing in the laboratory, and detailed trafficking studies hopefully will clarify which are the key cellular compartments in the trafficking process. Cathepsin C is known to be an activator of GrB (Pham and Ley, 1999), and the activation of Cathepsin C in MCF-7 cells after FGF-10 treatment (Fig. S4 A) fits well into our model. Although there are many future questions to be answered, including whether there is a functional nuclear localization signal in FGFR1, we have identified an entirely novel mechanism by which FGF signaling may regulate cancer cell behavior. Establishing the functional, prognostic, and therapeutic relevance of this new pathway in FGF signaling may prove critical for the development of new targeting strategies.

Materials and methods

Cell culture
MDA-MB-231 and MCF-7 cells were grown in DME without phenol red (Sigma-Aldrich) supplemented with 10% FBS (Biosera) and 4 mM L-glutamine (Cancer Research UK London Research Institute Cell Services). All cells were incubated at 37°C, 8% CO_2, and 100% relative humidity.

FGF-10 stimulation and inhibitor treatments
Cells (MDA-MB-231 or MCF-7) were seeded in DME without phenol red (with 10% FBS) either in 6-well plates (for protein extraction) or in 24-well plates (for immunocytochemistry) with 18-mm² coverslips (VWR International). The next day, medium was removed and replaced with serum-free medium containing 0.1% BSA (Sigma-Aldrich). Cells, at 70% confluency, were serum-starved overnight. For inhibitor experiments, cells were treated for 1 h with the FGFR inhibitor PD173074 (2 µM; Sigma-Aldrich) before stimulation with 100 ng/ml FGF-10 (PeproTech) and 300 ng/ml heparin sodium salt (Sigma-Aldrich) for different time points depending on the experiment.

RT-PCR and real-time RT-PCR
Extraction of total RNA was performed using an RNeasy kit (QIAGEN). All samples were treated with DNase on spin columns. Synthesis of cDNA was performed using reverse transcription (Superscript II; Invitrogen). RT-PCR was performed using PCR mastermix (MegaMix blue; Cambio). Real-time RT-PCR was performed using SYBR green RT-PCR kit (QuantiTect; QIAGEN) and using expression of *HPRT* and *GAPDH* as housekeeping genes for normalization with a melting curve performed after each reaction.

Primers for the promoter region of genes identified by ChIP on chip were designed using the sequences from the peak from the chip analysis after ChIP with FGFR1 antibody (Santa Cruz Biotechnology, Inc.). See next paragraph for primer pairs used for PCR and real-time RT-PCR. For Real-time RT-PCR, the threshold amplification cycles were determined using a real-time PCR machine (StepOnePlus; Applied Biosystems) and analyzed by the $2^{-\Delta\Delta Ct}$ method (Livak and Schmittgen, 2001).

The following primer pairs were used for PCR and real-time RT-PCR (annealing temperature [T_a] for all primers was 60°C unless otherwise stated): *EBI3* (promoter sequence) forward, 5'-GGGAGAGGGGAACAG-AAAAA-3', and reverse, 5'-CCTCTCCCTGTTCTTGCAACT-3'; EBI3 forward, 5'-ATTGCAACCTCTCTGCCTGT-3', and reverse, 5'-CGGTGACATTGA-GCACGTAG-3'; FGF-10 forward, 5'-ATGTCCGCTGGAGAAAGCTA-3', and reverse, 5'-CCTCTCCTTGGAGCTCCTTT-3'; FGFR1b forward, 5'-TTAATA-GCTCGGATGCGGAG-3', and reverse, 5'-ACGCAGACTGGTTAGCTTCA-3'; *GAPDH* (promoter sequence) forward, 5'-TACTAGCGGTTTTACGGGCG-3',

and reverse, 5'-CGAACAGGAGGAGCAGAGAGCGA-3'; GAPDH forward, 5'-CAATGACCCCTTCATTGACC-3', and reverse, 5'-TTGATTTT-GGAGGGATCTCG-3'; *GRINA* (promoter sequence) forward, 5'-TGAAG-CCGCTGAGGTTAAGT-3', and reverse, 5'-GTGCGACACTGACAGG-AGAA-3'; GRINA forward, 5'-GCTCTTCATCTTCGCCATTC-3', and reverse, 5'-CAGCGCAGCAAACACATACT-3'; HPRT forward, 5'-GACCAGTCAA-CAGGGGACAT-3', and reverse, 5'-CCTGACCAAGGAAACGAAAG-3'; *KRTAP5-6* (promoter sequence; T_a, 62°C) forward, 5'-GCCTAGCGAGA-AGTGACAGG-3', and reverse, 5'-ATGAGCGGTTTGTCTCTGGT-3'; KRTAP5-6 forward, 5'-AGCCCTGCTACTGTTCCTCA-3', and reverse, 5'-GGACTCACCTGAGGTCCAAA-3'; *MARK3* (promoter sequence) forward, 5'-CTCCCTGCTCCTGAATCTTG-3', and reverse, 5'-CATGATGCCC-ATTCACTCTG-3'; MARK3 forward, 5'-TCCTGTGCAGATGAACAACC-3', and reverse, 5'-ATTGCAACCTCTCTGCCTGT-3'; *POU2F2* (promoter sequence) forward, 5'-TGAGCTTCCCTGTCATTTCC-3', and reverse, 5'-GAA-GGGAGGAGGATTTGGAG-3'; POU2F forward, 5'-CCTGCTCAGTTCCT-GCTACC-3', and reverse, 5'-TCCAGCTCCTCCAGATCACT-3'; *PRSS27* (promoter sequence; T_a, 55°C) forward, 5'-TTTGAACAGAACTGCGGATG-3', and reverse, 5'-TGGGAGTCTTCCCCCTCTAT-3'; PRSS27 forward, 5'-CTTT-GAGACGGGCATGAACT-3', and reverse, 5'-CCAAACTCGGTGTCTTT-GCT-3'; *SFN* (promoter sequence; T_a, 62°C) forward, 5'-GCCAGGCT-GATCTCAAACTC-3', and reverse, 5'-GCTGAGAGGGAACAGCAATC-3'; SFN forward, 5'-GTCTGATCCAGAAGGCCAAG-3', and reverse, 5'-TGAGA-GCAGGTTTCGCTCTT-3'; *STAC3* (promoter sequence) forward, 5'-ACCC-AACTTGCATCTGCTTC-3', and reverse, 5'-ATGCCACAGTCATGGAGTCA-3'; and STAC3 forward, 5'-GGGCTTCGCTGTAAGAACTG-3', and reverse, 5'-GCGTACTGCTGGTTGCTGTA-3'.

Western blotting
Cell lysates were prepared using radioimmunoprecipitation assay buffer (Millipore) containing 1 mM NaF, 1 µg/ml aprotinin, 1 µg/ml leupeptin, 1 µg/ml pepstatin, and 1 mM PMSF (all obtained from Sigma-Aldrich), and the protein yield was determined using a Bradford dye binding assay (Bio-Rad Laboratories). Equivalent amounts of protein from different lysate samples (60 µg/well) were resolved by gel electrophoresis using precast 4–12% Bis-Tris mini gels (NuPAGE Novex; Invitrogen). After transferring proteins onto a nitrocellulose membrane (Whatman) overnight at 4°C at 12 V, membranes were blocked for 1 h at RT in 5% milk/PBS. Primary antibodies were diluted in 3% BSA/PBS and incubated overnight at 4°C. All antibodies were rabbit polyclonal unless otherwise stated: anti–α-tubulin antibody (mouse monoclonal; 1:2,000; Sigma-Aldrich), anti-Akt1/PKB-α (1:1,000; Millipore), anti-BIP/GRP78 (mouse monoclonal; 1:1,000; BD), anti–Cathepsin C (mouse monoclonal; D-6; 1:600; Santa Cruz Biotechnology, Inc.), anti-FGFR1 (1:1,000; SC-121; Santa Cruz Biotechnology, Inc.), anti-GrB antibody (1:1,000; Cell Signaling Technology), anti–HSC-70 (mouse monoclonal; 1:2,000; Santa Cruz Biotechnology, Inc.), anti–Lamin A/C (goat polyclonal; 1:600; sc-6215; Santa Cruz Biotechnology, Inc.), anti-MAPK1/2 (mouse monoclonal; 1:1,000; Millipore), anti-pAkt (1:1,000; Cell Signaling Technology), anti-pFRS2(Tyr196) (1:1,000; Cell Signaling Technology), anti-pERK (1:1,000; Cell Signaling Technology), anti–PLC-γ1 (1:1,000; Cell Signaling Technology), anti–pPLC-γ1 (1:1,000; Cell Signaling Technology), and anti-TOPOIIα (1:1,000; Santa Cruz Biotechnology, Inc.).

All secondary antibodies conjugated with HRP were obtained from Dako, and they were diluted in 3% BSA/PBS. Blots were incubated for 1 h at RT and were developed with ECL (GE Healthcare). All washes after the primary and the secondary antibodies were performed in 0.1% Tween 20/PBS for 3× for 5 min. Densitometric analysis was performed using ImageJ 1.429 software (National Institutes of Health). Signal density was normalized to the anti–α-tubulin or anti-HSC70 antibody as a loading control/reference for at least three separate treatments.

Migration assay
10^5 cells were plated onto 8-µm-pore Transwell migration filters in 24-well plates (Corning). Cells transfected with FGF-10 or empty vector were used 48 h after transfection. Cells were incubated either in DME supplemented with 4 mM L-glutamine and 1–10% FBS gradient or in DME supplemented with 0.1% BSA and with 4 mM L-glutamine without FBS overnight (12 h). The bottom of the Transwell was coated with 10 µg/ml fibronectin (Sigma-Aldrich) for 1 h at 37°C before plating the cells. 100 ng/ml FGF-10 (+300 ng/ml heparin) or 10 ng/ml EGF (Sigma-Aldrich) was added to the bottom of the Transwell as necessary. In the case of GrB inhibition, cells were pretreated with 25 µM GrB inhibitor before the migration assay as well as during (both in the top and bottom compartment of the Transwell) for 24 h in total.

Cells treated with siRNA were used 48 h after transfection. The cells were plated in serum-free medium with 0.1% BSA and with medium containing 10% FBS at the bottom of the Transwell. The bottom of the Transwell was coated with fibronectin as described previously in this paper.

Cells that had migrated to the lower surface were trypsinized. Similarly, cells from the upper chamber, which had not migrated, were removed with a cotton bud or trypsinized and counted separately. When treatments had an effect on cell number during the course of the migration assay (as a result of changes in either apoptosis and/or proliferation), the percentage of cell migration was calculated by normalizing the number of cells that migrated through the Transwell to the total cell number in the upper and lower chambers. The cell number was determined using an automatic cell counter (CASY; Schärfe System).

Proliferation assay

5×10^4 cells were plated in a 24-well plate in DME supplemented with 4 mM L-glutamine and 0.1% BSA with or without the presence of 100 ng/ml FGF-10 (and 300 ng/ml heparin). Cells were trypsinized and counted after 12, 24, and 48 h as described previously in this paper.

Immunofluorescence

All materials were obtained from Sigma-Aldrich unless otherwise stated. Cells on coverslips were fixed in 4% PFA in PBS for 15–20 min at RT and washed 3× for 5 min in PBS. Cells were permeabilized in 0.1% saponin/PBS at RT for 10 min and washed once with PBS. After blocking for 1 h at RT with 5% BSA/PBS, cells were incubated with primary antibody diluted in 3% BSA/PBS for 1 h at RT.

After incubation with primary antibody, cells were washed 3× for 5 min in PBS and then incubated with a secondary antibody conjugated with FITC (goat anti–rabbit IgG (H+L)-FITC; 1:100; Invitrogen) or Cy3 (donkey anti–mouse IgG-Cy3; 1:500; Jackson ImmunoResearch Laboratories, Inc.; Stratech Scientific) and diluted in 3% BSA/PBS for 1 h at RT. Finally, cells were washed again in PBS 3× for 5 min, and a final wash with H$_2$O was performed before mounting on slides using aqueous mounting media containing DAPI (Vectashield; Vector Laboratories).

For OCs, 4-µm paraffin sections were first dewaxed in xylene, rehydrated through a graded ethanol series, and collected in PBS followed by microwaving (900 W) in 10 mM sodium citrate buffer, pH 6.0, for 20 min. Sections were washed three times with PBS for 1 min each. Subsequent staining was performed as described previously in this paper.

Primary antibodies used were as follows: anti–α-tubulin (mouse; 1:2,000; reactivity: mouse and human; Sigma-Aldrich), anti–FGF-10 (goat; 1:1,000; Abcam), anti-FGFR1 (rabbit; 1:100; ab10646; Abcam), anti-FGFR1 (rabbit; 1:100; SC-121), anti-GrB (monoclonal mouse; 1:40; Novocastra Laboratories), anti-Ki67 (rabbit; 1:100; Abcam), and anti-NESO (rabbit; 1:100; gift from M. Djamgoz, Imperial College London, London, England, UK).

OC

This was modified from previously published protocols (Nyström et al., 2005; Chioni et al., 2010). 3.48 mg/ml collagen type I (Millipore) and Matrigel (BD) were mixed in a ratio of 70:30 (80% of final gel volume), 10× Hank's buffer (10% final gel volume) was added to the mix, and pH was adjusted to 7.4 with 2 M NaOH. Human foreskin fibroblasts (American Type Culture Collection) were resuspended in FBS (10% final gel volume) at 5×10^5/ml and added to the mix. The final mixture was applied to a 24-well plate (1 ml/well) and incubated at 37°C and 8% CO$_2$ for 4 h, after which the gels were equilibrated by immersion in medium for 16 h, whereupon the medium was replaced by 500 µl culture medium containing 10^6 MDA-MB-231 cells. 250 µl collagen mix (7 vol collagen type I, 1 vol each of 10× Hank's buffer, FBS, and culture medium neutralized with 2 M NaOH) was added dropwise onto 400-mm^2 Nylon membranes (100-µm pore; Tetko, Inc.). Membranes were incubated at 37°C for 30 min and then fixed for 1 h at 4°C with 1% glutaraldehyde (Sigma-Aldrich)/PBS. After fixation, the membranes were washed 4× for 5 min in PBS and incubated overnight in culture medium at 4°C. The coated membranes were placed on 25-mm^2 sterile stainless steel grids in 6-well plates. Gels were lifted from the 24-well plate and laid on top of the coated membranes. An appropriate amount of culture medium was added to each well until it reached the lower part of the gel, so that the cultures were maintained at the air–liquid interface. In the case of treatment with 2 µM PD173074 inhibitor, fresh inhibitor was added to the medium at each medium change. In all cases, medium was changed every 2 d, and after 10 d, the gels were fixed in 4% PFA (Sigma-Aldrich) for 16 h at 4°C. After fixation, gels were washed thoroughly in PBS, bisected, and dehydrated through a graded ethanol series before wax embedding.

Immunofluorescence of OCs for optical projection tomography

OCs were fixed in 4% PFA overnight at 4°C and then washed for 30 min in PBS. Samples were dehydrated stepwise in methanol with PBS diluent (33, 66, and 100% methanol for ≥15 min at each step). The samples were incubated at −80°C three to five times for ≥1 h each time and back to RT to ensure that antigens in the deeper parts of the tissue were rendered accessible. Tissues were then rehydrated in a series of 0.1% Tween 20/PBS (PBST) with methanol as diluent (33, 66, and 100% for 15 min at each step). Tissues were blocked in 10% BSA/PBS for 24 h at 4°C and then incubated with primary antibody (rabbit anti-NESO at 1:100 dilution) and diluted in 1.5 ml blocking solution containing 5% DMSO for 48 h at 4°C. After 4× 30-min washes with PBST, samples were incubated with secondary antibody (1:100; goat anti–rabbit Alexa Fluor 488 antibody; Invitrogen) and diluted in 1.5 ml blocking solution containing 5% DMSO for 48 h at 4°C followed by washing with PBST 4× for 30 min. Finally, samples were fixed in 4% PFA overnight at 4°C and then washed in PBST 5× for 30 min. The samples were then sent to Bioptonics (Medical Research Council Technology) for optical projection tomography.

Subcellular fractionation

MCF-7 and MDA-MB-231 cells were plated in T25 flasks (VWR International), and subcellular fractionation was performed using a subcellular protein fractionation kit (PerkinElmer). In the case of FGF-10 and/or GrB treatment, fractionation was performed using a different kit (Universal Magnetic Co-IP kit; Active Motif) because of the discontinuation of the previous kit.

GrB inhibitor treatment

5×10^4 cells were plated in a 24-well plate in DME supplemented with 4 mM L-glutamine and 10% FBS. The next day, cells were treated with 25 or 50 µM GrB synthetic peptide inhibitor (Caspase-8 inhibitor II; EMD; Martin et al., 1998) for 12, 24, and 48 h and then fixed with 4% PFA for subsequent staining for FGFR1. In the case of cotreatment with FGF-10/heparin, cells were treated with 25 µM GrB inhibitor for 24 h in DME supplemented with 4 mM L-glutamine and 0.1% BSA. After 24 h of treatment, FGF-10 was added as described previously in this paper for 1–2 h. Alternatively, MCF-7 cells were treated for 5 h with 50 µM DCI (Enzo Life Sciences), a serine protease inhibitor (Harper et al., 1985), and then fixed as described previously in this paper.

RNAi

siRNA used (Thermo Fisher Scientific) were as follows: Genome SMARTpool for human FGFR1 (M-003131) and human GrB (M-005889). For silencing FGFR1 target genes, the following ON-TARGETplus siRNA SMARTpools were used: human PRSS27 (L-005971), human SFN (L-005180), human GRINA (L-010697), human EBI3 (L-012093), and human KRTAP5-6 (L-033250). Cells (40–50% confluent in 6-well plates) were transfected for 4 h with 10 nM siRNA using 4 µl INTERFERin (Polyplus Transfection; PeqLab) in a total reaction volume of 1.1 ml in each well of a 6-well plate. mRNAs, proteins, and functional activity were assayed 48–72 h after transfection and compared with mock and/or control siRNA-treated cells (siCONTROL Non-Targeting siRNA pool D-001210 or ON-TARGETplus Non-Targeting Pool D-001810; Thermo Fisher Scientific). Transfection efficiency was assessed independently using a positive control siRNA Lamin A/C (D-001050; Thermo Fisher Scientific), which was compared with the siCONTROL nontargeting siRNA.

Cloning FGFR1b and IC-FGFR1b

Full-length human FGFR1b cloned into SalI and BamHI sites of the pBluescript KS II (+) vector was a gift from S. Werner (Eidgenössische Technische Hochschule Zürich, Zürich, Switzerland). Full-length human FGFR1b was subcloned into the BamHI and XhoI sites of the pcDNA4/TO mammalian expression vector (Invitrogen).

The IC-FGFR1 was amplified from our full-length FGFR1b construct using cloning PCR primers tagged with c-MYC epitope and containing engineered EcoRI and HindIII recognition sites. The PCR product was cloned into the HindIII and EcoRI sites of pcDNA4/TO. The following sequences were used: hFGFR1-IC forward, 5′-CACAAGCTTAAGATGAAGAGTGGTACCAAGAAGAGTGACTTCCACAGCC-3′, and hFGFR1-full length reverse c-MYC tag, 5′-GCCGAATTCTCACAGATCTTCTTCAGAAATAAGTTTTTGTTCGCGGCGTTTGAGTCCGCCATTGGC-3′. Cells were transfected with 1 µg DNA using 3 µl Lipofectamine 2000 (Invitrogen) for 4 h.

Site-directed mutagenesis

The mutant FGFR1b-VSAN was generated from full-length human FGFR1b in pcDNA4/TO using site-directed mutagenesis (QuikChange II XL; Agilent Technologies), the mutagenesis primer 5′-CAGACAGGTAACAGTGTCT-GCTAACTCCAGTGCATCCATGAACTC-3′, and its reverse complement.

Immunohistochemistry

Paraffin-embedded sections were dewaxed in xylene and rehydrated through graded ethanols to PBS. Antigen retrieval was performed by microwaving (900 W) in 10 mM sodium citrate buffer, pH 6.0, for 20 min followed by 3× 1-min washes with PBS. DAB staining was performed using the Vectastain elite ABC kit (Vector Laboratories). In brief, samples were treated with hydrogen peroxide (0.3% in H_2O) for 30 min at RT and then blocked in normal serum/PBS for 15 min at RT (150 µl FBS/10 ml PBS). The sections were incubated with primary antibody (in serum/PBS as described previously in this paper) for 1 h at RT. After washing 3× in PBS, they were incubated with the secondary antibody (50 µl secondary antibody in 10 ml serum/PBS) for 30 min at RT and washed again in PBS as previously in this paper. They were then incubated in ABC solution for 30 min at RT and washed 3× in PBS. The sections were then developed by using DAB substrate kit for peroxidase kit (Vector Laboratories) and incubated for 1–5 min (FGFR1 for 1 min [Abcam]; FGFR1 for 4 min [Santa Cruz Biotechnology, Inc.]). Sections were washed for 5 min in H_2O and then counterstained with hematoxylin for 2 min and finally washed in tap water. Sections were dehydrated through graded ethanols to xylene before mounting in di-N-butyle phthalate in xylene (Sigma-Aldrich).

Breast human tissues were provided by L. Jones (Barts Cancer Institute, London, England, UK). Tissues from breast cancer ($n = 11$) and normal breast ($n = 10$) were stained for FGFR1. Primary antibodies were used as follows: Abcam FGFR1 (rabbit pAb; catalog no. ab10646; 1:1500) and Santa Cruz Biotechnology, Inc. FGFR1 (rabbit pAb Flag c-15; catalog no. SC-121; 1:750).

ChIP on chip analysis

ChIP (ChIP kit; Millipore) and subsequent chip analysis were performed to identify putative involvement of FGFR1 in transcriptional regulation. In brief, MCF-7 cells were used as starting material, with chromatin cross-linked by fixation in 1% formaldehyde for 10 min at 37°C before cell lysis. Approximately 10^6 cells were lysed in 200 µl SDS lysis buffer, and the DNA was sheared by sonication (4× 10-s sonication; 30% amplitude with 30-s break between each round; Vibra-Cell; Sonics and Materials, Inc.) to a mean length of ∼500 bp. The range of DNA fragment size was confirmed by reversing the cross-links with 8 µl of 5-M NaCl in 200 µl cell lysate at 65°C for 4 h, recovering the DNA by phenol/chloroform extraction, and electrophoresing the sample on a 1% agarose/TBE (Tris-borate-EDTA) gel. The sonicated cell lysate was diluted 10-fold in ChIP dilution buffer, and 1% of the diluted DNA was kept as the input control for subsequent PCR analysis. Histones were precleaned with salmon sperm DNA/protein A agarose 50% slurry for 1 h at 4°C with agitation. Precleaned chromatin was immunoprecipitated with 2 µg anti-FGFR1 antibody (SC-121), anti–RNA polymerase II antibody (positive control; Millipore), or IgG1 control (BD) overnight at 4°C with constant rotation. The antibody–histone complex was collected by adding salmon sperm DNA/protein A agarose slurry (30% of the total sample volume) for 1 h at 4°C with constant rotation. The samples were washed and eluted. Both the immunoprecipitated and the control input samples (each in 500-µl volume) were then subjected to cross-link reversal, adding 10 µl of 0.5-M EDTA, 20 µl of 1-M Tris-HCl, pH 6.5, and 2 µl of 10-mg/ml proteinase K, and incubating for 1 h at 45°C. DNA was recovered by phenol/chloroform extraction and ethanol precipitation.

Eight different chromatin samples were immunoprecipitated with FGFR1 antibody, and five were immunoprecipitated with an IgG control. One sample immunoprecipitated with RNA polymerase II was used as a positive control. Samples were amplified by whole-genome amplification (WGA2 kit; Sigma-Aldrich). Library preparations were performed using the whole chromatin immunoprecipitated sample (resuspended in 10 µl water). However, in the case of the input control, 10 ng of each sample was diluted with water to a final volume of 10 µl. In each sample, 2 µl of Library preparation buffer and 1 µl Library stabilization solution were added and incubated at 95°C for 2 min. Samples were cooled on ice and spun briefly, and 1 µl Library preparation enzyme was added. Samples were incubated as follows: at 16°C for 20 min, at 24°C for 20 min, at 37°C for 20 min, at 75°C for 5 min, and final hold at 4°C before two rounds of amplification. For the first round, 7.5 µl of 10× amplification master mix, 47.5 µl nuclease-free water, and 5 µl WGA DNA polymerase was added to each tube, and samples were subjected to the following

cycle: 95°C for 3 min, 20 cycles of 94°C for 15 s, 65°C for 5 min, and then a final hold at 4°C. Samples were purified using PCR clean up columns (QIAquick; QIAGEN). A second amplification step was performed using 15 ng of purified amplified product, as described previously in this paper, for a further 20 cycles. Samples were then sent to NimbleGen (Roche) for chip analysis. An initial selection of putative targets was made by grouping the Excel (Microsoft) datasets returned from NimbleGen. Samples, which appeared in at least three of the FGFR1 samples and none of the IgG controls, were considered for further analysis.

GrB activity assay

GrB activity was assayed using the chromogenic substrate Ac-IEPD-pNA (Enzo Life Sciences) to directly measure GrB activity in cell lysates. As a positive control experiment, recombinant human GrB (Enzo Life Sciences) was added to the reaction buffer at 3, 6, and 12 U/µl according to the manufacturer's instructions. Furthermore, the serine protease inhibitor DCI (50 µM) was added to assay buffer together with 6 U recombinant GrB to confirm that it blocked GrB activity. To measure GrB activity in MCF-7 cells, 5×10^5 cells were seeded in 6-well plates and, upon reaching 70% confluence, were serum starved overnight before treatment with 100 ng/ml FGF-10 for the appropriate time. When appropriate, they were preincubated with 50 µM DCI for 1 h before FGF-10 treatment. They were then lysed in 150 µl mammalian protein extraction reagent (Thermo Fisher Scientific) according to the manufacturer's instructions. Four independent experiments were performed, each in triplicate using 50 µl cell lysate for each replicate. The colorimetric reaction was started by adding 200 µM Ac-IEPD-pNA substrate to each sample and monitoring absorbance at 405 nm continuously in a plate reader (Spectra MR; Dynex Technologies).

Data analysis

All quantitative data are presented as means ± standard errors, unless stated otherwise. Statistical significance was determined with Student's t test, Mann–Whitney rank sum, or analysis of variance (ANOVA) test as appropriate.

Real-time PCR data were analyzed using the $2^{-\Delta\Delta Ct}$ method (Livak and Schmittgen, 2001). Results were considered significant at $P < 0.05$. Unless otherwise stated, all experiments were performed a minimum of three independent times each in triplicate.

Cell invasion in the OCs and nuclear staining of FGFR1 in the confocal images were analyzed using ImageJ 1.429 software. Cell invasion index was calculated using the area of the invading particles, the depth of invasion, and the number of invading particles. Four different OCs were analyzed for each condition, and each time, a whole transverse section through the center of the organotypic was used for analysis. To calculate FGFR1 staining in the nucleus, DAPI staining was used as a marker to define the nuclear area, and at least five random images from three independent experiments were analyzed.

Microscope image acquisition

Confocal images were acquired at RT using a confocal microscope (LSM710 Axio Observer.Z1; Carl Zeiss). Images were taken using the following objectives, magnifications, and numerical aperture: (a) Plan-Apochromat, 63×, 1.40 oil differential interference contrast M27; (b) Plan Apochromat, 40×, 1.3 oil differential interference contrast M27; and (c) EC Plan Neofluar, 20×, 0.50 M27. Immersol 518 F (Carl Zeiss) was used as an imaging medium when required. The acquisition software used was ZEN 2008 (Carl Zeiss).

Bright-field images were acquired at RT using a light microscope (Axiophot; Carl Zeiss) connected to a camera (AxioCam HRz; Carl Zeiss). The objectives used were all Plan Neofluar with magnification and numerical aperture as follows: (a) 63×, 1.25 oil; (b) 40×, 0.75; (c) 20×, 0.5; (d) 10×, 0.3; and (e) 5×, 0.15. Immersol 518 F was used as an imaging medium when required. The acquisition software used was AxioVision Release 4.8 (Carl Zeiss).

Online supplemental material

Fig. S1 shows the specificity of the FGFR1 antibody that has been used in this study. Fig. S2 shows that GrB inhibitor treatment blocked FGFR1 nuclear localization and RNAi-mediated knockdown of GrB reduced migration in MCF-7 cells. Fig. S3 shows validation of our GrB activity assay before assaying GrB activity in cell lysates. Fig. S4 shows effect of FGF-10 stimulation on Cathepsin C and GrB protein levels and validation of ChIP on chip results by independent ChIP. Fig. S5 confirms successful overexpression of FGFR1b and mRNA expression levels of FGFR1 target genes after RNAi-mediated knockdown of GrB or transient transfection of IC-FGFR1. Video 1 shows optical projection tomography of a 3D organotypic

References

Adam, R.M., T. Danciu, D.L. McLellan, J.G. Borer, J. Lin, D. Zurakowski, M.H. Weinstein, P.H. Rajjayabun, J.K. Mellon, and M.R. Freeman. 2003. A nuclear form of the heparin-binding epidermal growth factor-like growth factor precursor is a feature of aggressive transitional cell carcinoma. *Cancer Res.* 63:484–490.

Badea, L., V. Herlea, S.O. Dima, T. Dumitrascu, and I. Popescu. 2008. Combined gene expression analysis of whole-tissue and microdissected pancreatic ductal adenocarcinoma identifies genes specifically over-expressed in tumor epithelia. *Hepatogastroenterology.* 55:2016–2027.

Bray, S.J. 2006. Notch signalling: a simple pathway becomes complex. *Nat. Rev. Mol. Cell Biol.* 7:678–689. http://dx.doi.org/10.1038/nrm2009

Bryant, D.M., and J.L. Stow. 2005. Nuclear translocation of cell-surface receptors: lessons from fibroblast growth factor. *Traffic.* 6:947–954. http://dx.doi.org/10.1111/j.1600-0854.2005.00332.x

Bryant, D.M., F.G. Wylie, and J.L. Stow. 2005. Regulation of endocytosis, nuclear translocation, and signaling of fibroblast growth factor receptor 1 by E-cadherin. *Mol. Biol. Cell.* 16:14–23. http://dx.doi.org/10.1091/mbc.E04-09-0845

Buzza, M.S., L. Zamurs, J. Sun, C.H. Bird, A.I. Smith, J.A. Trapani, C.J. Froelich, E.C. Nice, and P.I. Bird. 2005. Extracellular matrix remodeling by human granzyme B via cleavage of vitronectin, fibronectin, and laminin. *J. Biol. Chem.* 280:23549–23558. http://dx.doi.org/10.1074/jbc.M412001200

Carpenter, G., and H.J. Liao. 2009. Trafficking of receptor tyrosine kinases to the nucleus. *Exp. Cell Res.* 315:1556–1566. http://dx.doi.org/10.1016/j.yexcr.2008.09.027

Chioni, A.M., and R. Grose. 2008. Organotypic modelling as a means of investigating epithelial-stromal interactions during tumourigenesis. *Fibrogenesis Tissue Repair.* 1:8. http://dx.doi.org/10.1186/1755-1536-1-8

Chioni, A.M., and R. Grose. 2009. Negative regulation of fibroblast growth factor 10 (FGF-10) by polyoma enhancer activator 3 (PEA3). *Eur. J. Cell Biol.* 88:371–384. http://dx.doi.org/10.1016/j.ejcb.2009.01.004

Chioni, A.M., S.P. Fraser, F. Pani, P. Foran, G.P. Wilkin, J.K. Diss, and M.B. Djamgoz. 2005. A novel polyclonal antibody specific for the Na(v)1.5 voltage-gated Na(+) channel 'neonatal' splice form. *J. Neurosci. Methods.* 147:88–98. http://dx.doi.org/10.1016/j.jneumeth.2005.03.010

Chioni, A.M., D. Shao, R. Grose, and M.B. Djamgoz. 2010. Protein kinase A and regulation of neonatal Nav1.5 expression in human breast cancer cells: activity-dependent positive feedback and cellular migration. *Int. J. Biochem. Cell Biol.* 42:346–358. http://dx.doi.org/10.1016/j.biocel.2009.11.021

Corson, L.B., Y. Yamanaka, K.M. Lai, and J. Rossant. 2003. Spatial and temporal patterns of ERK signaling during mouse embryogenesis. *Development.* 130:4527–4537. http://dx.doi.org/10.1242/dev.00669

Dailey, L., D. Ambrosetti, A. Mansukhani, and C. Basilico. 2005. Mechanisms underlying differential responses to FGF signaling. *Cytokine Growth Factor Rev.* 16:233–247. http://dx.doi.org/10.1016/j.cytogfr.2005.01.007

D'Eliseo, D., P. Pisu, C. Romano, A. Tubaro, C. De Nunzio, S. Morrone, A. Santoni, A. Stoppacciaro, and F. Velotti. 2010. Granzyme B is expressed in urothelial carcinoma and promotes cancer cell invasion. *Int. J. Cancer.* 127:1283–1294. http://dx.doi.org/10.1002/ijc.25135

Devergne, O., M. Hummel, H. Koeppen, M.M. Le Beau, E.C. Nathanson, E. Kieff, and M. Birkenbach. 1996. A novel interleukin-12 p40-related protein induced by latent Epstein-Barr virus infection in B lymphocytes. *J. Virol.* 70:1143–1153.

Dunham-Ems, S.M., Y.W. Lee, E.K. Stachowiak, H. Pudavar, P. Claus, P.N. Prasad, and M.K. Stachowiak. 2009. Fibroblast growth factor receptor-1 (FGFR1) nuclear dynamics reveal a novel mechanism in transcription control. *Mol. Biol. Cell.* 20:2401–2412. http://dx.doi.org/10.1091/mbc.E08-06-0600

Elbauomy Elsheikh, S., A.R. Green, M.B. Lambros, N.C. Turner, M.J. Grainge, D. Powe, I.O. Ellis, and J.S. Reis-Filho. 2007. FGFR1 amplification in breast carcinomas: a chromogenic in situ hybridisation analysis. *Breast Cancer Res.* 9:R23. http://dx.doi.org/10.1186/bcr1665

Eswarakumar, V.P., I. Lax, and J. Schlessinger. 2005. Cellular signaling by fibroblast growth factor receptors. *Cytokine Growth Factor Rev.* 16:139–149. http://dx.doi.org/10.1016/j.cytogfr.2005.01.001

Fang, X., E.K. Stachowiak, S.M. Dunham-Ems, I. Klejbor, and M.K. Stachowiak. 2005. Control of CREB-binding protein signaling by nuclear fibroblast growth factor receptor-1: a novel mechanism of gene regulation. *J. Biol. Chem.* 280:28451–28462. http://dx.doi.org/10.1074/jbc.M504400200

Hanneken, A. 2001. Structural characterization of the circulating soluble FGF receptors reveals multiple isoforms generated by secretion and ectodomain shedding. *FEBS Lett.* 489:176–181. http://dx.doi.org/10.1016/S0014-5793(00)02409-1

Harper, J.W., K. Hemmi, and J.C. Powers. 1985. Reaction of serine proteases with substituted isocoumarins: discovery of 3,4-dichloroisocoumarin, a new general mechanism based serine protease inhibitor. *Biochemistry.* 24:1831–1841. http://dx.doi.org/10.1021/bi00329a005

Ho, A., and S.F. Dowdy. 2002. Regulation of G(1) cell-cycle progression by oncogenes and tumor suppressor genes. *Curr. Opin. Genet. Dev.* 12:47–52. http://dx.doi.org/10.1016/S0959-437X(01)00263-5

Hu, S.X., S. Wang, J.P. Wang, G.B. Mills, Y. Zhou, and H.J. Xu. 2003. Expression of endogenous granzyme B in a subset of human primary breast carcinomas. *Br. J. Cancer.* 89:135–139. http://dx.doi.org/10.1038/sj.bjc.6601051

Hu, Y., X. Fang, S.M. Dunham, C. Prada, E.K. Stachowiak, and M.K. Stachowiak. 2004. 90-kDa ribosomal S6 kinase is a direct target for the nuclear fibroblast growth factor receptor 1 (FGFR1): role in FGFR1 signaling. *J. Biol. Chem.* 279:29325–29335. http://dx.doi.org/10.1074/jbc.M311144200

Kermorgant, S., and P.J. Parker. 2008. Receptor trafficking controls weak signal delivery: a strategy used by c-Met for STAT3 nuclear accumulation. *J. Cell Biol.* 182:855–863. http://dx.doi.org/10.1083/jcb.200806076

Kumar, K.N., N. Tilakaratne, P.S. Johnson, A.E. Allen, and E.K. Michaelis. 1991. Cloning of cDNA for the glutamate-binding subunit of an NMDA receptor complex. *Nature.* 354:70–73. http://dx.doi.org/10.1038/354070a0

Levi, E., R. Fridman, H.Q. Miao, Y.S. Ma, A. Yayon, and I. Vlodavsky. 1996. Matrix metalloproteinase 2 releases active soluble ectodomain of fibroblast growth factor receptor 1. *Proc. Natl. Acad. Sci. USA.* 93:7069–7074. http://dx.doi.org/10.1073/pnas.93.14.7069

Li, C., M. Iida, E.F. Dunn, A.J. Ghia, and D.L. Wheeler. 2009a. Nuclear EGFR contributes to acquired resistance to cetuximab. *Oncogene.* 28:3801–3813. http://dx.doi.org/10.1038/onc.2009.234

Li, W., D.M. Danilenko, S. Bunting, R. Ganesan, S. Sa, R. Ferrando, T.D. Wu, G.A. Kolumam, W. Ouyang, and D. Kirchhofer. 2009b. The serine protease marapsin is expressed in stratified squamous epithelia and is up-regulated in the hyperproliferative epidermis of psoriasis and regenerating wounds. *J. Biol. Chem.* 284:218–228. http://dx.doi.org/10.1074/jbc.M806267200

Lin, S.Y., K. Makino, W. Xia, A. Matin, Y. Wen, K.Y. Kwong, L. Bourguignon, and M.C. Hung. 2001. Nuclear localization of EGF receptor and its potential new role as a transcription factor. *Nat. Cell Biol.* 3:802–808. http://dx.doi.org/10.1038/ncb0901-802

Livak, K.J., and T.D. Schmittgen. 2001. Analysis of relative gene expression data using real-time quantitative PCR and the 2(-Delta Delta C(T)) Method. *Methods.* 25:402–408. http://dx.doi.org/10.1006/meth.2001.1262

Lo, H.W., S.C. Hsu, M. Ali-Seyed, M. Gunduz, W. Xia, Y. Wei, G. Bartholomeusz, J.Y. Shih, and M.C. Hung. 2005a. Nuclear interaction of EGFR and STAT3 in the activation of the iNOS/NO pathway. *Cancer Cell.* 7:575–589. http://dx.doi.org/10.1016/j.ccr.2005.05.007

Lo, H.W., W. Xia, Y. Wei, M. Ali-Seyed, S.F. Huang, and M.C. Hung. 2005b. Novel prognostic value of nuclear epidermal growth factor receptor in breast cancer. *Cancer Res.* 65:338–348.

Loeb, C.R., J.L. Harris, and C.S. Craik. 2006. Granzyme B proteolyzes receptors important to proliferation and survival, tipping the balance toward apoptosis. *J. Biol. Chem.* 281:28326–28335. http://dx.doi.org/10.1074/jbc.M604544200

Maher, P.A. 1996. Nuclear translocation of fibroblast growth factor (FGF) receptors in response to FGF-2. *J. Cell Biol.* 134:529–536. http://dx.doi.org/10.1083/jcb.134.2.529

Małecki, J., A. Wiedłocha, J. Wesche, and S. Olsnes. 2002. Vesicle transmembrane potential is required for translocation to the cytosol of externally added FGF-1. *EMBO J.* 21:4480–4490. http://dx.doi.org/10.1093/emboj/cdf472

Martin, D.A., R.M. Siegel, L. Zheng, and M.J. Lenardo. 1998. Membrane oligomerization and cleavage activates the caspase-8 (FLICE/MACHalpha1) death signal. *J. Biol. Chem.* 273:4345–4349. http://dx.doi.org/10.1074/jbc.273.8.4345

Mohammadi, M., S. Froum, J.M. Hamby, M.C. Schroeder, R.L. Panek, G.H. Lu, A.V. Eliseenkova, D. Green, J. Schlessinger, and S.R. Hubbard. 1998. Crystal structure of an angiogenesis inhibitor bound to the FGF receptor tyrosine kinase domain. *EMBO J.* 17:5896–5904. http://dx.doi.org/10.1093/emboj/17.20.5896

Myers, J.M., G.G. Martins, J. Ostrowski, and M.K. Stachowiak. 2003. Nuclear trafficking of FGFR1: a role for the transmembrane domain. *J. Cell. Biochem.* 88:1273–1291. http://dx.doi.org/10.1002/jcb.10476

Navarro, J.M., J. Casatorres, and J.L. Jorcano. 1995. Elements controlling the expression and induction of the skin hyperproliferation-associated keratin K6. *J. Biol. Chem.* 270:21362–21367. http://dx.doi.org/10.1074/jbc.270.36.21362

Nyström, M.L., G.J. Thomas, M. Stone, I.C. Mackenzie, I.R. Hart, and J.F. Marshall. 2005. Development of a quantitative method to analyse tumour cell invasion in organotypic culture. *J. Pathol.* 205:468–475. http://dx.doi.org/path.1716

Ornitz, D.M., and N. Itoh. 2001. Fibroblast growth factors. *Genome Biol.* 2: reviews3005.1–reviews3005.12. http://dx.doi.org/10.1186/gb-2001-2-3-reviews3005

Peng, H., J. Moffett, J. Myers, X. Fang, E.K. Stachowiak, P. Maher, E. Kratz, J. Hines, S.J. Fluharty, E. Mizukoshi, et al. 2001. Novel nuclear signaling pathway mediates activation of fibroblast growth factor-2 gene by type 1 and type 2 angiotensin II receptors. *Mol. Biol. Cell.* 12:449–462.

Peng, H., J. Myers, X. Fang, E.K. Stachowiak, P.A. Maher, G.G. Martins, G. Popescu, R. Berezney, and M.K. Stachowiak. 2002. Integrative nuclear FGFR1 signaling (INFS) pathway mediates activation of the tyrosine hydroxylase gene by angiotensin II, depolarization and protein kinase C. *J. Neurochem.* 81:506–524. http://dx.doi.org/10.1046/j.1471-4159.2002.00833.x

Pham, C.T., and T.J. Ley. 1999. Dipeptidyl peptidase I is required for the processing and activation of granzymes A and B in vivo. *Proc. Natl. Acad. Sci. USA.* 96:8627–8632. http://dx.doi.org/10.1073/pnas.96.15.8627

Reilly, J.F., and P.A. Maher. 2001. Importin β–mediated nuclear import of fibroblast growth factor receptor: role in cell proliferation. *J. Cell Biol.* 152:1307–1312. http://dx.doi.org/10.1083/jcb.152.6.1307

Reilly, J.F., E. Mizukoshi, and P.A. Maher. 2004. Ligand dependent and independent internalization and nuclear translocation of fibroblast growth factor (FGF) receptor 1. *DNA Cell Biol.* 23:538–548. http://dx.doi.org/10.1089/dna.2004.23.538

Reis-Filho, J.S., P.T. Simpson, N.C. Turner, M.B. Lambros, C. Jones, A. Mackay, A. Grigoriadis, D. Sarrio, K. Savage, T. Dexter, et al. 2006. FGFR1 emerges as a potential therapeutic target for lobular breast carcinomas. *Clin. Cancer Res.* 12:6652–6662. http://dx.doi.org/10.1158/1078-0432.CCR-06-1164

Shiba-Ishii, A., J. Kano, Y. Morishita, Y. Sato, Y. Minami, and M. Noguchi. 2011. High expression of stratifin is a universal abnormality during the course of malignant progression of early-stage lung adenocarcinoma. *Int. J. Cancer.* 129:2445–2453. http://dx.doi.org/10.1002/ijc.25907

Sorokin, A., M. Mohammadi, J. Huang, and J. Schlessinger. 1994. Internalization of fibroblast growth factor receptor is inhibited by a point mutation at tyrosine 766. *J. Biol. Chem.* 269:17056–17061.

Stachowiak, M.K., P.A. Maher, A. Joy, E. Mordechai, and E.K. Stachowiak. 1996a. Nuclear accumulation of fibroblast growth factor receptors is regulated by multiple signals in adrenal medullary cells. *Mol. Biol. Cell.* 7:1299–1317.

Stachowiak, M.K., P.A. Maher, A. Joy, E. Mordechai, and E.K. Stachowiak. 1996b. Nuclear localization of functional FGF receptor 1 in human astrocytes suggests a novel mechanism for growth factor action. *Brain Res. Mol. Brain Res.* 38:161–165. http://dx.doi.org/10.1016/0169-328X(96)00010-1

Stachowiak, M.K., P.A. Maher, and E.K. Stachowiak. 2007. Integrative nuclear signaling in cell development—a role for FGF receptor-1. *DNA Cell Biol.* 26:811–826. http://dx.doi.org/10.1089/dna.2007.0664

Thornberry, N.A., T.A. Rano, E.P. Peterson, D.M. Rasper, T. Timkey, M. Garcia-Calvo, V.M. Houtzager, P.A. Nordstrom, S. Roy, J.P. Vaillancourt, et al. 1997. A combinatorial approach defines specificities of members of the caspase family and granzyme B. Functional relationships established for key mediators of apoptosis. *J. Biol. Chem.* 272:17907–17911. http://dx.doi.org/10.1074/jbc.272.29.17907

Turner, N., and R. Grose. 2010. Fibroblast growth factor signalling: from development to cancer. *Nat. Rev. Cancer.* 10:116–129. http://dx.doi.org/10.1038/nrc2780

Turner, N., A. Pearson, R. Sharpe, M. Lambros, F. Geyer, M.A. Lopez-Garcia, R. Natrajan, C. Marchio, E. Iorns, A. Mackay, et al. 2010. FGFR1 amplification drives endocrine therapy resistance and is a therapeutic target in breast cancer. *Cancer Res.* 70:2085–2094. http://dx.doi.org/10.1158/0008-5472.CAN-09-3746

Wang, S.C., H.C. Lien, W. Xia, I.F. Chen, H.W. Lo, Z. Wang, M. Ali-Seyed, D.F. Lee, G. Bartholomeusz, F. Ou-Yang, et al. 2004. Binding at and transactivation of the COX-2 promoter by nuclear tyrosine kinase receptor ErbB-2. *Cancer Cell.* 6:251–261. http://dx.doi.org/10.1016/j.ccr.2004.07.012

Wang, Y.N., H. Yamaguchi, J.M. Hsu, and M.C. Hung. 2010. Nuclear trafficking of the epidermal growth factor receptor family membrane proteins. *Oncogene.* 29:3997–4006. http://dx.doi.org/10.1038/onc.2010.157

Wiedłocha, A., P.O. Falnes, I.H. Madshus, K. Sandvig, and S. Olsnes. 1994. Dual mode of signal transduction by externally added acidic fibroblast growth factor. *Cell.* 76:1039–1051. http://dx.doi.org/10.1016/0092-8674(94)90381-6

Xia, W., Y. Wei, Y. Du, J. Liu, B. Chang, Y.L. Yu, L.F. Huo, S. Miller, and M.C. Hung. 2009. Nuclear expression of epidermal growth factor receptor is a novel prognostic value in patients with ovarian cancer. *Mol. Carcinog.* 48:610–617. http://dx.doi.org/10.1002/mc.20504

Xie, H., T. Turner, M.H. Wang, R.K. Singh, G.P. Siegal, and A. Wells. 1995. In vitro invasiveness of DU-145 human prostate carcinoma cells is modulated by EGF receptor-mediated signals. *Clin. Exp. Metastasis.* 13:407–419. http://dx.doi.org/10.1007/BF00118180

Xie, Y., and M.C. Hung. 1994. Nuclear localization of p185neu tyrosine kinase and its association with transcriptional transactivation. *Biochem. Biophys. Res. Commun.* 203:1589–1598. http://dx.doi.org/10.1006/bbrc.1994.2368

Zammit, C., R. Barnard, J. Gomm, R. Coope, S. Shousha, C. Coombes, and C. Johnston. 2001. Altered intracellular localization of fibroblast growth factor receptor 3 in human breast cancer. *J. Pathol.* 194:27–34. http://dx.doi.org/10.1002/path.846

Zhang, X., O.A. Ibrahimi, S.K. Olsen, H. Umemori, M. Mohammadi, and D.M. Ornitz. 2006. Receptor specificity of the fibroblast growth factor family. The complete mammalian FGF family. *J. Biol. Chem.* 281:15694–15700. http://dx.doi.org/10.1074/jbc.M601252200